JGR Atmospheres

RESEARCH ARTICLE
10.1029/2019JD031823

Special Section:
Atmospheric Rivers: Intersection of Weather and Climate

Contribution of Atmospheric Rivers to Annual, Seasonal, and Extreme Precipitation Across British Columbia and Southeastern Alaska

A. R. Sharma[1] and S. J. Déry[2]

[1]Natural Resources and Environmental Studies Program, University of Northern British Columbia, Prince George, British Columbia, Canada, [2]Environmental Science and Engineering Program, University of Northern British Columbia, Prince George, British Columbia, Canada

Abstract Lying in the frontline of the prevailing midlatitude westerlies, British Columbia and southeastern Alaska (BCSAK) often receive copious amounts of precipitation through atmospheric rivers (ARs). This study quantifies the contribution of ARs to annual, seasonal, and extreme precipitation across BCSAK from 1979 to 2012 using a recently developed high-resolution gridded precipitation data set, a regional AR catalog, and integrated vapor transport fields calculated from a reanalysis data set. On average, ARs contribute 13% of total annual precipitation with the higher contribution along the coastal regions (up to 33%), parts of which are one of the wettest locations on Earth, followed by the Columbia and Rocky Mountains (~9%–15%). The highest contributions occur during September (up to 57%) and October (up to 49%). The contribution of ARs to extreme precipitation attains >90% along the western arc of the Coast Mountains and the coastal regions of BCSAK. ARs act as the main synoptic-scale mechanism that brings rainfall to the Rocky Mountains in winter. The probability of observing AR-related precipitation increases over the study period; however, no change occurs in the average AR-related precipitation amount for most of BCSAK during 1979–2012. This work provides insights on the critical role ARs play on the water resources of northwestern North America and has broader implications on community water supply and management, hydropower operations, and flood risk assessment and mitigation.

Key Points:
- Up to 33% of annual precipitation derives from atmospheric rivers (ARs) in coastal British Columbia and SE Alaska (BCSAK)
- ARs contribute <5% to >90% of annual extreme precipitation in BCSAK; higher contributions occur in elevated terrain
- Higher AR-related precipitation occurs during September (up to 57%) and October (up to 49%) across BCSAK, 1979–2012

Supporting Information:
- Supporting Information S1

Correspondence to:
A. R. Sharma,
asharma@unbc.ca

Citation:
Sharma, A. R., & Déry, S. J. (2020). Contribution of atmospheric rivers to annual, seasonal, and extreme precipitation across British Columbia and southeastern Alaska. *Journal of Geophysical Research: Atmospheres*, *123*. https://doi.org/10.1029/2019JD031823

Received 14 OCT 2019
Accepted 4 APR 2020
Accepted article online 16 APR 2020

1. Introduction

Globally, the regions exposed to westerly maritime flows receive a substantial amount of their precipitation and its extremes from extratropical cyclones, mostly during the cold season (Gimeno et al., 2012; Hawcroft et al., 2012). British Columbia (BC), Canada and southeastern Alaska (AK), the United States (BCSAK), lies in the frontline of the prevailing midlatitude westerlies and receive copious amounts of precipitation, especially during autumn and winter, primarily through the extratropical cyclones emanating from the North Pacific (Hare, 1998; Stahl et al., 2006). Although westerlies dominate this region's climate, the presence of steep topography leads to enhanced precipitation through the orographic uplift of moisture within transient Pacific extratropical cyclones (Neiman et al., 2008). Atmospheric rivers (ARs), the phenomenon first identified by Zhu and Newell (1994) to represent the filamentary structure of atmospheric water vapor transport, are long (>2,000 km) and narrow (length/width >2) mesoscale synoptic corridors of moisture often found in the warm sector of the extratropical cyclones (Lavers et al., 2011; Ralph et al., 2004, 2017). Generally concentrated in the lower troposphere, these moisture conveyor belts produce effectively orographic precipitation when they interact with mountain topography and influence substantially the precipitation of western North America including BCSAK (Dettinger et al., 2011; Ralph et al., 2005, 2013).

Through their cumulative effects, ARs influence substantially seasonal precipitation anomalies, short-term weather and flooding events, and contribute exceptionally to the global water cycle; indeed, they transport >90% of (sub)tropical moisture poleward at midlatitudes globally (Ralph et al., 2017; Zhu & Newell, 1998). Owing to the importance of ARs in water vapor transport inland and their impacts on water resources and extreme hydrological events, there exist extensive studies on the identification and characteristics of ARs (Bao et al., 2006; Guan & Waliser, 2015; Lavers et al., 2012; Neiman et al., 2008; Ralph et al., 2004), impacts on precipitation (Chen et al., 2018; Dettinger et al., 2011; Lavers et al., 2013; Lavers & Villarini, 2015; Rutz

et al., 2014), snow accumulation (Goldenson et al., 2018; Gorodetskaya et al., 2014), and peak runoff and flooding (Curry et al., 2019; Konrad & Dettinger, 2017; Ralph et al., 2006).

During an AR, conditions are conducive to the occurrence of heavy orographic precipitation (Neiman et al., 2008; Ralph et al., 2013). A moist low-level jet, large water vapor content, strong horizontal winds propagating toward the elevated terrain, and steep mountains yield heavy orographic precipitation from ARs (Lin et al., 2001; Neiman et al., 2002). Moreover, the strength of orographic precipitation associated with an AR depends on different variables such as terrain elevation, slope, wind speed and direction, and the orientation of the AR trajectory (Lin et al., 2001; Neiman et al., 2008; Ralph et al., 2003). The proximity of an area to the coast and presence (or absence) of a topographic barrier also influence the AR-related precipitation in that area. This arises owing to the depletion of water vapor over the topographic barrier that leads to AR decay farther inland (Rutz et al., 2014).

Precipitation associated with ARs varies in terms of amount and phase based on factors such as the time of the year, elevation, latitude, and proximity to the coast. Generally, an intense AR-related precipitation event occurs along the windward side of coastal mountains and weakens further inland (Rutz et al., 2015). The intense precipitation from an AR replenishes freshwater resources and occasionally leads to extreme flooding (e.g., the September 2010 Bella Coola, BC flood event; PCIC, 2013). In this context, the literature lacks the quantification and characterization of the precipitation and its extremes associated with ARs across BCSAK. Moreover, an increase in the global surface air temperature intensifies the availability of atmospheric moisture in-line with the Clausius-Clapeyron relation (Dessler et al., 2008). This, in turn, causes an increase in the horizontal moisture transport through ARs (Lavers et al., 2015; Payne & Magnusdottir, 2015; Radić et al., 2015). However, it is not yet known whether there have been recent increases or decreases in the contribution of ARs to precipitation across BCSAK. Motivated by these research gaps, this study aims to analyze the relationship between ARs and precipitation in this region. We explore changes in the fractional contribution of ARs to precipitation over recent decades with an implementation of a zero-inflated beta regression model. Specifically, the main objectives of this work are (i) to quantify the contribution of landfalling ARs to annual and seasonal precipitation (including its partitioning into rainfall and snowfall), to assess changes in contributions during 1979–2012 across BCSAK, and (ii) to understand the relationship between ARs and extreme precipitation across BCSAK during 1979–2012.

2. Study Area

The BCSAK region covers an area of ~1.07 × 10^6 km^2 (BC ~0.95 × 10^6 km^2 and southeastern AK ~0.12 × 10^6 km^2) with latitudes ranging from ~47.5°N to 60.0°N, longitudes spanning from 114.0°W to 139.0°W, and elevations varying from sea level to >4,000 m (Figure 1). Much of the western Canadian Cordillera lies within this region and forms a barrier to the midlatitude prevailing westerlies (Hare, 1998; Moore et al., 2010). BCSAK includes temperate rainforests, montane and alpine environments, a flat interior plateau, wet western slopes, and dry rain-shadow regions (Church & Ryder, 2010; Holland, 1976). Its weather shows a distinct climatological pattern controlled by season, the proximity to the coast, and topography, such as a modest (coast) to high (inland) annual air temperature range. A strong precipitation gradient with a moist coastal region and dry interior occurs due to the presence of the Coast Mountains and their rain-shadow effect (Moore et al., 2010; O'Neel et al., 2015). The Columbia and Rocky Mountains to the east, the Coast and Insular Mountains to the west, and the St. Elias Mountains to the north of BCSAK form headwaters of many major rivers of western Canada and the Pacific Coast including the Columbia, Fraser, Mackenzie, Nass, Skeena, Stikine, and Yukon Rivers (Hernández-Henríquez et al., 2017; Reynoldson et al., 2005; Richardson & Milner, 2005).

3. Data and Methods

3.1. Data

3.1.1. Precipitation Data

We use daily gridded precipitation from the Pacific Climate Impacts Consortium meteorology for northwestern North America (PNWNAmet) data set (Werner et al., 2019). PNWNAmet is a high-resolution meteorological data set recently developed by Pacific Climate Impacts Consortium, available through their data portal: https://www.pacificclimate.org/data/daily-gridded-meteorological-datasets; accessed 17 August

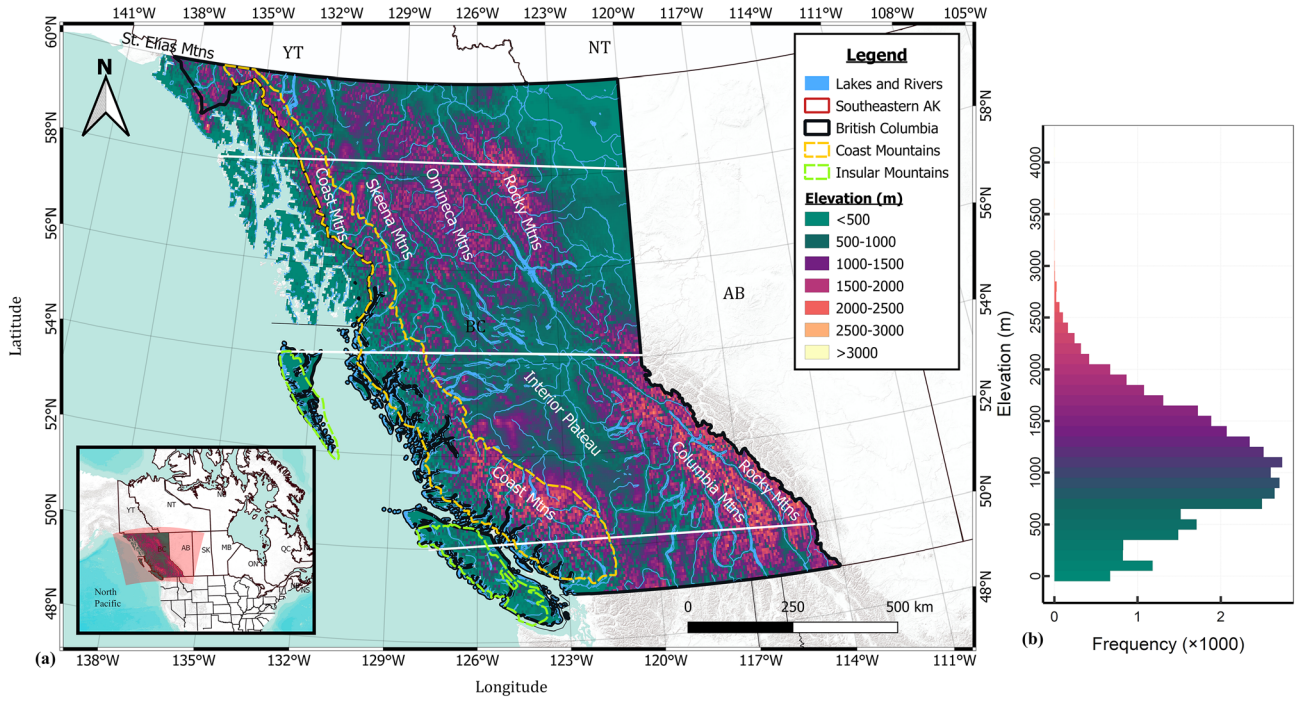

Figure 1. (a) Map of BCSAK showing the elevation, lakes, rivers, and major mountain ranges. The straight white solid lines near 50°N, 54°N, and 58°N parallels depict the transects from the coast to inland, for which the AR contribution change inland is extracted (Figure 9). (b) Distribution of different elevation ranges in bins of 100 m within the study area at 0.0625° × 0.0625° resolution (same as that of gridded precipitation data).

2018. This data set provides temporally consistent daily gridded precipitation and daily minimum and maximum air temperatures at a relatively high spatial resolution of 0.0625° × 0.0625° (~6 km × 6 km) for northwestern North America spanning 1 January 1945 to 31 December 2012. Werner et al. (2019) constructed the PNWNAmet daily gridded data using three independent variables as predictors: longitude, latitude, and Climate Western North America (ClimateWNA; v5.10) monthly climate normals (Wang et al., 2006, 2016). The ClimateWNA data set, available at monthly temporal resolution, implements a bilinear interpolation and an elevation adjustment to generate scale-free climate data for western Canada and the Alaska Panhandle (Wang et al., 2006, 2016).

Werner et al. (2019) perform validation of the PNWNAmet and other available gridded data (e.g., Natural Resources Canada meteorology [NRCANmet], also known as the Australian National University Spline; McKenney et al., 2011) with the independent Agricultural and Rural Development Act network data, of which many stations were located at elevations >1,000 m above sea level throughout BC covering 1965 to 1991. Their results show that the PNWNAmet precipitation has a lower magnitude positive bias when compared to the negative bias shown by NRCANmet precipitation (see Figure 2a in Werner et al., 2019). For average and extreme precipitation, PNWNAmet outperforms NRCANmet making it a more reliable product for the higher end of extreme precipitation analysis compared to other major daily frequency gridded products for this region (Werner et al., 2019). For example, the biases of PNWNAmet and NCARmet versus Agricultural and Rural Development Act for total annual precipitation when daily precipitation amount is >95th percentile are −4.25% and −30.71%, respectively (Werner et al., 2019). We calculate the total monthly, seasonal, and annual precipitation from the daily data and average these values over the period of study.

Daily precipitation partitioning into snow and rain relies on daily mean air temperature (obtained as the average of daily minimum and maximum air temperatures) threshold following the UBC Watershed Model equation (Quick & Pipes, 1977). This model considers the precipitation as all snow when daily mean air temperature ≤0.6 °C and all rain if ≥3.6 °C. Equation (1) then gives the proportion of snow when daily mean air temperature (T, °C) lies between 0.6 °C and 3.6 °C (Kienzle, 2008; Quick & Pipes, 1977; Trubilowicz & Moore, 2017):

$$\text{Snow proportion} = 1 - \left(\frac{T}{3} - 0.2\right). \quad (1)$$

This approach, originally designed and validated for mountainous catchments in BC (e.g., the Columbia and Fraser river basins; Quick & Pipes, 1977), considers the thermal energy distribution and the gradual change from rain to snow based on a linear transition.

3.1.2. Data on ARs

Given the significance of ARs in water resources and their accompanying extreme weather events, many AR databases have been developed in recent years that provide information on AR chronologies and characteristics at global and regional levels, including the BCSAK region (Gershunov et al., 2017; Guan & Waliser, 2015; Rutz et al., 2014). We use the AR chronology and integrated vapor transport (IVT) information in BCSAK from a 6-hourly AR catalog published by the Scripps Institution of Oceanography (SIO-R1-AR catalog, Gershunov et al., 2017; http://cw3e.ucsd.edu/Publications/SIO-R1-Catalog/, accessed 13 February 2018). The IVT field is regridded using bilinear interpolation to the resolution of the PNWNAmet data set. This AR catalog provides the frequency, duration, and landfalling location, along with IVT gridded data at 6-hourly temporal resolution across the North American West Coast (20°N to 60°N) from January 1948 to March 2017. The SIO-R1-AR catalog was derived using the 6-hourly specific humidity and wind fields at 2.5° × 2.5° spatial resolution from the National Centers for Environmental Prediction/National Center for Atmospheric Research (NCEP/NCAR) reanalysis data set (Kalnay et al., 1996). Gershunov et al. (2017) validated the SIO-R1-AR catalog by comparing it against the Special Sensor Microwave Imager-based AR catalog recorded by Neiman et al. (2008) and observed a favorable comparison between these two data sets.

Given the substantial modulation of precipitation amounts by ocean-atmosphere climate variability, we explore how the contributions of ARs to precipitation across BCSAK differ during alternating Pacific Decadal Oscillation (PDO) and El Niño–Southern Oscillation (ENSO) phases. The PNWNAmet data set provides the precipitation during the cool phase of the PDO (1948–1976) for comparison with its warm phase (1977–1999) (Mantua & Hare, 2002). Similarly, the multivariate ENSO index provides years with ENSO phases (Wolter & Timlin, 2011). The Mann-Whitney-Wilcoxon test provides statistical significance of the distribution of AR-related precipitation during different phases of ENSO (Hollander et al., 2014).

3.2. Methods

3.2.1. The Contribution of ARs to Precipitation

A calculation of the fraction of precipitation attributed to ARs determines their contribution to total annual and seasonal precipitation for January 1979 to December 2012. Reasons for selecting this study period are to (i) minimize the precipitation variability associated with PDO phases (see sections 4.7 and 5.2; Meehl et al., 2009) and (ii) obtain an improved representation of the AR chronology and IVT field through the ingestion of remote sensing data into the NCEP/NCAR reanalysis after 1979 (Kalnay et al., 1996). To calculate the fraction of AR-related precipitation, we first derive the chronology of landfalling AR-days and the following day in BCSAK (47.5°N to 60.0°N), called AR-days, from the SIO-R1-AR catalog. Consideration of both the landfalling AR day and the following day addresses the 1-day uncertainty between the Coordinated Universal Time-based AR chronology and the local time gridded precipitation data (Dettinger et al., 2011). Next, for each grid cell, the precipitation is AR-related if the IVT is ≥250 kg m^{-1} s^{-1} for these AR-days. Then, a division of the AR-related precipitation by total precipitation for each grid cell provides the fraction of the contribution of ARs to the precipitation. The coefficient of variation (CV = standard deviation (SD)/Mean) provides the interannual variability on the contribution of ARs to annual precipitation across BCSAK.

We obtain annual and seasonal extreme precipitation for each grid cell across BCSAK following the block maxima approach of the statistical method of extreme value theory (Coles, 2001; Lavers & Villarini, 2013). This approach provides one extreme precipitation event per year for 1979–2012, creating a series of 34 events for each grid cell across BCSAK. The block maxima, a widely used approach for extreme event analysis (e.g., Blanchet et al., 2009; Lavers & Villarini, 2013), minimizes serial dependence of extreme precipitation events and covers longer temporal ranges. Next, for each year, we cross-reference the annual extreme day with the AR-days series and if there is a match, it is considered an AR-influenced extreme occurrence. Thereafter, a

division of the number of AR-influenced extreme occurrences by the number of total extreme events provides the fraction of the AR-related extreme precipitation in each grid cell across BCSAK. The same approach provides the fractional contribution of ARs to seasonal extreme precipitation occurrences using results for autumn: September–November, winter: December–February, spring: March–May, and summer: June–August, in place of the annual values.

3.2.2. Zero-Inflated Beta Regression and Logistic Regression Models

An implementation of the zero-inflated beta regression model gives the temporal change on the contribution of ARs to total precipitation over 1979–2012 across BCSAK. Beta regression models, an extension of generalized linear models, describe rates and proportions in situations where the response is constrained to the open interval (0,1) (Ferrari & Cribari-Neto, 2004; Ospina & Ferrari, 2010). In AR contribution time series, however, the response results may contain zeros; therefore, we implement the zero-inflated beta distribution that allows zero and the fractional values, that is, an interval of [0,1) (Ospina & Ferrari, 2010). For a random variable y_i (AR fraction in ith year) the zero-inflated beta distribution is given as (Lavers & Villarini, 2015; Ospina & Ferrari, 2010):

$$\begin{cases} f(y_i) = \nu, \text{ if } y_i = 0, \\ f(y_i|\mu,\sigma) = (1-\nu)\dfrac{\Gamma(\sigma)}{\Gamma(\mu\sigma)\Gamma((1-\mu)\sigma)} y_i^{\mu\sigma}\,(1-y_i)^{((1-\mu)\sigma)-1} \text{ if } y_i \in (0,\,1) \end{cases} \tag{2}$$

where $\Gamma(.)$ is the gamma function, the parameters μ, σ, and ν represent the mean, variance, and the probability of a zero observation, respectively, and satisfy $0 < \mu < 1$, $\sigma > 0$, and $0 < \nu < 1$. Equations (3) and (4) provide the expected value and variance, respectively:

$$E(y_i) = (1-\nu)\mu, \tag{3}$$

$$\mathrm{Var}(y_i) = (1-\nu)\left(\frac{\mu(1-\mu)}{\sigma+1}\right) + \nu(1-\nu)\mu^2. \tag{4}$$

The generalized additive models for location, scale, and shape (gamlss) package in R provides tools to implement the highly flexible zero-inflated beta regression model in location, scale, and shape (Stasinopoulos & Rigby, 2007). The model reveals changes over time in the contribution of ARs to precipitation for each grid cell for the parameters μ, σ, and ν (Lavers & Villarini, 2015; Ospina & Ferrari, 2012). We consider all possible model combinations so that each parameter can be a linear function of time and select the model with the lowest Akaike Information Criterion (Akaike, 1974). The Akaike Information Criterion provides a compromise between the goodness-of-fit and complexity of the models.

An implementation of the logistic regression model yields the temporal change of the contribution of ARs to extreme precipitation. Let x_i be the covariate (presence or absence of an AR during an extreme precipitation day) for ith year, then the probability P of a binary response variable (y) to be 1 is given as (Fahrmeir et al., 2013):

$$P(y_i = 1) = \frac{e^{(\beta_0+\beta_1 x_i)}}{1+e^{(\beta_0+\beta_1 x_i)}} \text{ for } y_i \in (0,\,1), \tag{5}$$

where the logistic model coefficients β_0 and β_1 represent the intercept and rate of change in log-odd, respectively. These coefficients are estimated through the maximum likelihood method (Fahrmeir et al., 2013).

The change in contribution over time is significant at each grid cell if the probability value (p value) <0.05 for both the zero-inflated beta regression and logistic regression models.

To further evaluate the global significance of the individual grid-scale significant changes, we perform a field significance test following Wilks (2011, 2016) that minimizes the false discovery rate (FDR). If p_i with $i = 1, 2, \ldots, N$ denotes grid-scale p values for N hypothesis tests sorted in ascending order so that $p_{(1)} \le p_{(2)} \le \ldots \le p_{(N)}$ with p_1 being most significant and p_N least significant, then the results of individual tests are considered globally significant if their respective p values are no greater than a threshold level p_{FDR} that depends on the distribution of sorted p values as (Wilks, 2011, 2016):

$$p_{\mathrm{FDR}} = \max_{i=1,\,2,\,\ldots,\,N} \left[p_i : p_i \le \left(\frac{i}{N} \right) \alpha_{\mathrm{global}} \right] \tag{6}$$

where α_{global} is the chosen control level for the FDR, that is, 0.05 in this study.

4. Results

4.1. Precipitation Climatology

The average annual and monthly precipitation amounts across BCSAK reveal the distinct influence of mountains and proximity to the coast (Figures S1a and S2 in the supporting information). Average total annual precipitation maps show higher amounts (≥10,000 mm year^{-1}) along the western slopes of the Coast Mountains of BCSAK relative to their eastern counterparts (Figure S1a). This precipitation total approaches the value recorded in perhaps the world's wettest location, Cherrapunjee, northeastern India, which averages 11,987 ± 3324 mm of rainfall annually (Jain et al., 2013; Murata et al., 2007). This suggests that parts of coastal BCSAK lie amongst the wettest regions on the planet. Mountainous regions (e.g., the Columbia and Rocky Mountains, Figure 1a) of BCSAK receive moderate amounts (~1,500 mm year^{-1}) of annual precipitation. Moreover, there are drier regions with precipitation <500 mm year^{-1} in northeastern BC and parts of the central Interior Plateau owing to the rain-shadow effect on moisture-laden westerly flows (Figure S1a). The variability of total annual precipitation is lower along the coastal and mountainous regions of BCSAK; the average variation in precipitation is highest during August, February, and September and lowest during October, June, and May (Figures S1b and S3).

4.2. The Contribution of ARs to Total Precipitation

The contribution of ARs to total annual precipitation shows high spatial variability with contributions ranging from <5% to >33% (spatial average = 13%) across BCSAK during 1979–2012 (Figure 2a and Table 1). The highest contribution occurs in the low-lying coastal regions (~33%) followed by the mountainous terrain of BCSAK (Figure 2a). The contribution of ARs averages 20%, 11%, and 6% of total annual precipitation along the ranges of the Coast, Columbia, and Rocky Mountains, respectively (Table 2). These indicate average contributions over 34 years but exclude year-to-year variability. For example, the spatially averaged highest contribution occurs in 2005 (27%) (spatial range: 2%–45%) and the lowest occurs in 1982 (10%) (spatial range: 0%–26%). Furthermore, ARs contribute one third of the average ~10,000 mm year^{-1} precipitation in coastal regions whereas in northeastern BC the contribution is minimal because, on average, they contribute only a small fraction (~4% of the 600 mm year^{-1} total precipitation). The coefficient of variation of the percentage of the contribution of ARs to total annual precipitation reveals lower variability along the coastal regions of BCSAK (<0.2) that increases with inland distance from the coast to reach >1.0 along northeastern BC (Figure 2b).

The BCSAK region receives higher precipitation during autumn and winter months (up to 2,200 mm in a single month along the coastal region) and lower amounts during late spring and early summer months with some areas receiving no precipitation at all (Figure S2). Average total monthly precipitation associated with ARs ranges from no precipitation to >50% depending on the month and location within the region (Figure 3). The highest and most widespread contribution occurs during late summer and autumn (August: 3%–37%, September: 6%–57%, October: 2%–49%, and November: 0%–37%), whereas the lowest contribution occurs during spring months (Figure 3 and Table 1).

4.3. The Contribution of ARs to Extreme Precipitation

ARs contribute up to 97% of annual extreme precipitation in parts of BCSAK during 1979–2012 (Figure 4). The highest contribution of ARs to extreme precipitation lies along southeastern AK (up to 97%), Haida Gwaii (94%), Vancouver Island (~90%), coastal regions of central BC (up to ~90%), and the Columbia and Rocky Mountains (up to ~60%) (Figure 4). A seasonal analysis shows the highest contribution occurs during autumn (up to 82% in southeastern AK, ~75% in the Coast Mountains and the western arc from the Coast Mountains, and 50%–60% in the Columbia and Rocky Mountains), followed by winter (Figure S4). Similar to total annual and monthly precipitation, the influences of orography and proximity to the coast are visible in the AR-related extreme annual and seasonal precipitation. For example, the contribution of ARs to annual extreme precipitation diminishes to <10% toward northeastern BC likely because this region lies

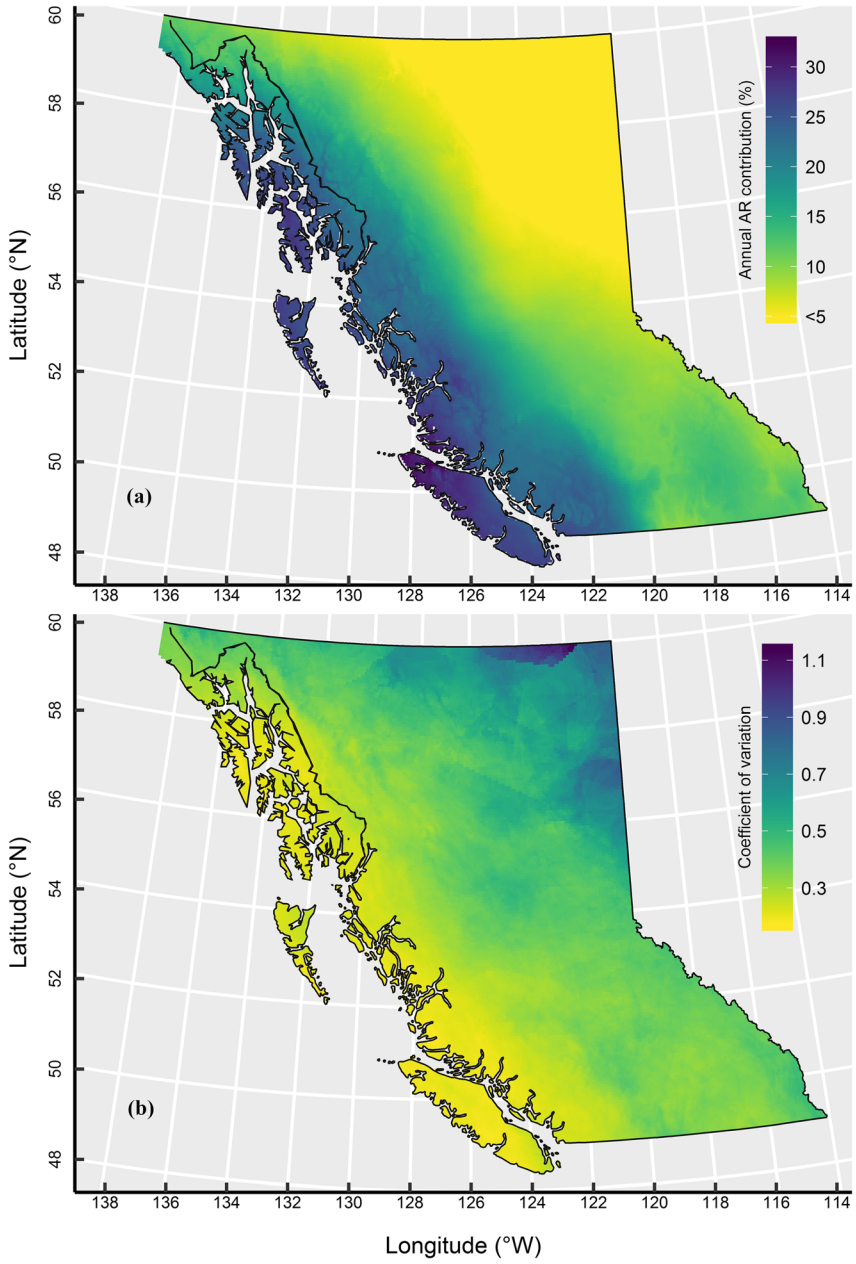

Figure 2. The (a) average of, and (b) coefficient of variation in, the contribution of ARs to total annual precipitation across BCSAK, 1979–2012.

in the lee of several prominent north-south mountain ranges and farther inland from the Pacific Ocean (Figure 4).

4.4. The Influence of ARs on Snowfall and Rainfall

A monthly and seasonal decomposition of the contribution of ARs to snowfall and rainfall indicates a higher AR association with liquid rather than solid precipitation across BCSAK during 1979–2012 (Table 1 and Figures 5–7). On average, ARs contribute 5 ± 4% (spatial range 0%–29%) of total snowfall during autumn and 6 ± 5% (spatial range 0%–22%) in winter; they contribute 48 ± 20% (spatial range 0%–100%) and 36 ± 11% (spatial range 5%–84%) of total rainfall during autumn and winter, respectively. A distinct variation occurs in the spatial distribution of the contribution of ARs to snowfall, and it exhibits an elevational dependency across BCSAK (Figures 6 and 7). The contribution of ARs to rainfall exceeds that for snowfall along

Table 1
Contribution of ARs to Total Annual and Monthly Precipitation (%), Snowfall (%), and Rainfall (%) Across BCSAK, 1979–2012

Period	Average contribution of ARs to precipitation (%) (spatial range [%])	Average contribution of ARs to snowfall (% of total snowfall) (spatial range [%])	Average contribution of ARs to rainfall (% of total rainfall) (spatial range [%])
January	10 (0–24)	7 (0–26)	56 (0–100)
February	7 (0–24)	5 (0–19)	36 (0–100)
March	4 (0–18)	2 (0–13)	13 (0–100)
April	5 (0–18)	2 (0–11)	8 (0–39)
May	5 (0–18)	1 (0–13)	6 (0–31)
June	5 (0–23)	1 (0–14)	5 (0–23)
July	9 (1–26)	1 (0–14)	9 (0–26)
August	15 (3–37)	1 (0–24)	15 (3–37)
September	24 (6–57)	1 (0–34)	26 (6–75)
October	23 (2–49)	6 (0–36)	35 (5–95)
November	14 (0–37)	8 (0–29)	47 (0–100)
December	10 (0–27)	7 (0–23)	53 (0–100)
Annual	13 (0–33)	7 (0–23)	18 (3–44)

the ranges of the Coast, Columbia, and Rocky Mountains of BCSAK (Table 2). Moreover, the higher percentage of AR-related rainfall is skewed toward the lower elevation ranges of BCSAK whereas that of snowfall is skewed toward mid-to-high elevation ranges (Figures 7 and S5). During autumn, the contribution of ARs to snowfall attains up to 29% but only at higher elevations of the Coast, Columbia, and Rocky Mountains, and remains <5% for most of BCSAK, especially at lower elevations (Figure 5a). However, the spatial extent of the contribution of ARs to snowfall increases in winter, influencing most of BCSAK except lower elevation, coastal regions, and parts of northeastern BC. In contrast, the average contribution of ARs to rainfall reaches up to 100%, especially in winter, suggesting that ARs constitute the only synoptic-scale mechanism inducing rainfall in the Coast and Rocky Mountains and northwestern BC during this season (Figure 5a). This may lead to rain-on-snow events especially in winter and early spring because ARs bring much warmer, moist air than seasonal averages.

A breakdown of the contribution of ARs to extreme precipitation into rainfall and snowfall also exhibits an elevational and seasonal dependency across BCSAK. During autumn, the contribution to extreme rainfall is greater than snowfall for most of BCSAK except at high elevations (Figures 5b and 6b). However, in winter the pattern changes with only coastal regions of BCSAK receiving extreme rainfall from ARs. For example, during autumn, ARs contribute on average 25% as extreme rainfall (up to 97% in southeastern AK and northern coastal BC, up to 70% in Vancouver Island and the Coast Mountains, ~65% along the Columbia and Rocky Mountains, ~50% along the coastal areas, and < 5% in northeastern BC) but only 6% as extreme snowfall especially along the higher elevation grid cells (~55% above 2,000 m in the Coast Mountains and ~60% above 1,500 m in the Columbia and Rocky Mountains).

4.5. The Inland Influence of ARs on Precipitation

The contribution of ARs to annual and monthly precipitation decreases gradually moving inland in BCSAK, but with variations across seasons and elevations (Figure 8). Longitudinal profiles of the contribution of ARs to precipitation near the 50°N, 54°N, and 58°N parallels from the Pacific coast up to the BC/Alberta border (Figure 1a) reveal on average a ~20%–30% contribution to total annual precipitation for up to ~300 km inland from the coast along all three transects (Figure 8). However, the contribution decreases gradually to <20% near the 50°N and 54°N parallels and <10% near the 58°N parallel within a distance of ~500 km inland from the coast.

ARs influence ~50–75% of extreme annual precipitation within the first 300 km inland from the coast at all three transects with an abrupt decrease to <30% in the Interior Plateau. At lower latitudes (e.g., the 50°N transect), the contribution of ARs to extreme annual precipitation exceeds 70% along the South Coast followed by ~45% across the Columbia and Rocky Mountains (Figure 8). Unlike the lower latitudinal transects, the contribution to extreme precipitation along the 58°N transect decreases and remains ~10% once reaching the northern Rocky Mountains. The eastward shift in the maxima of extreme precipitation as one proceeds southward from the 58°N parallel is due to the geography of the Coast Mountains that acts as a barrier to

Table 2
Average Contribution of ARs (%) to Annual Precipitation, Rainfall, and Snowfall Across the Coast, Columbia, and Rocky Mountains of BCSAK, 1979–2012

Phase of precipitation	Coast Mountains	Columbia Mountains	Rocky Mountains
Precipitation (%) (spatial range [%])	20 (9–28)	11 (8–14)	6 (3–14)
Rainfall (%) (spatial range [%])	32 (17–42)	13 (11–18)	9 (4–17)
Snowfall (%) (spatial range [%])	14 (3–23)	10 (3–13)	4 (0–11)

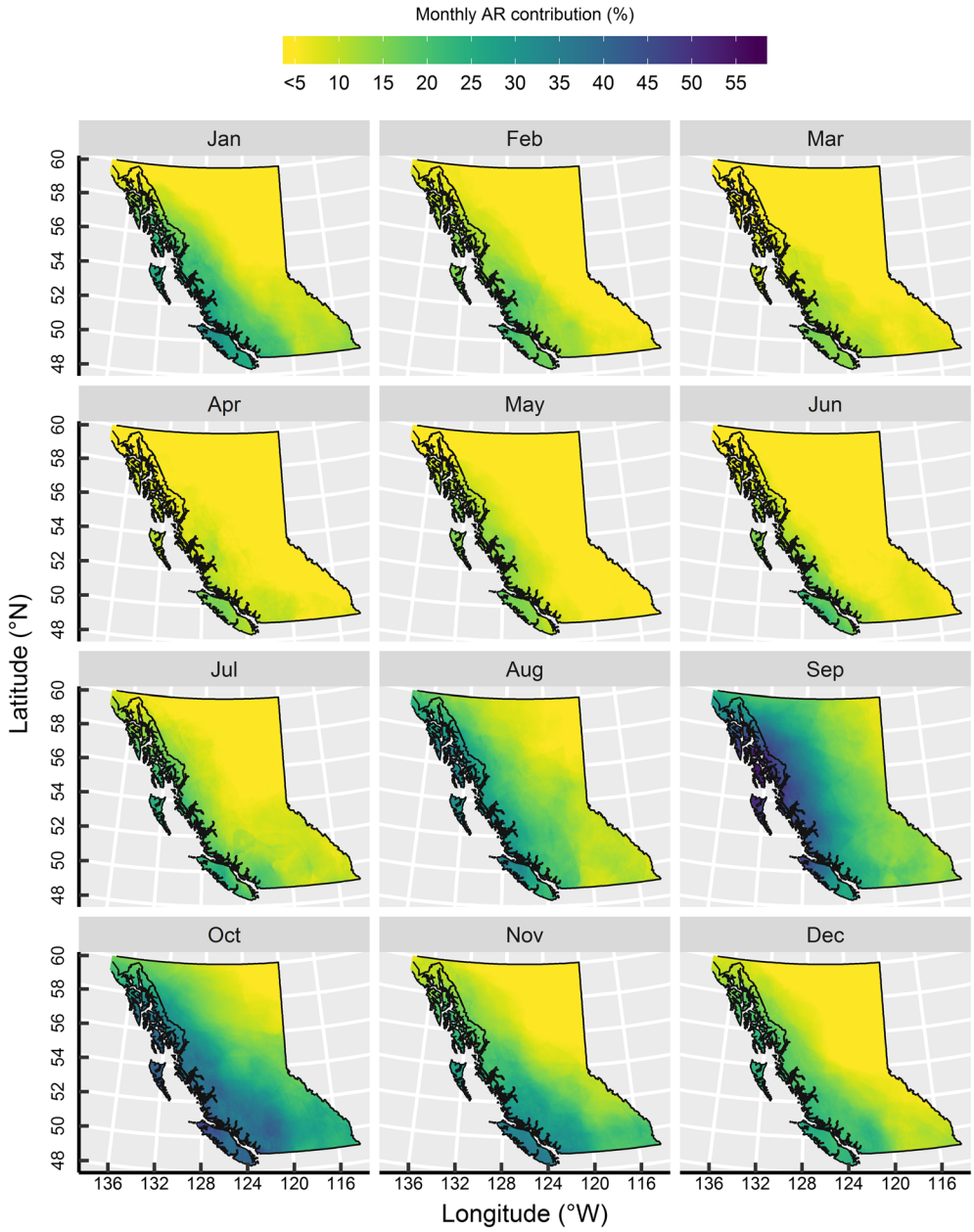

Figure 3. The BCSAK 1979–2012 average AR contribution to monthly precipitation (%).

further inland penetration of moisture carried by the ARs. Breaks in the Coast Mountains, presumably, cause a reduced magnitude of these gradients at 54°N. Moreover, an increase in AR-related precipitation maxima near the 50°N transect in the Interior Mountains is due to the orographic barriers that enhance the uplift of moisture-laden ARs resulting in greater precipitation totals, mostly on the windward side.

4.6. Temporal Change in the Contribution of ARs to Precipitation

With a 13% (spatial range <5–33%) spatially averaged contribution to total annual precipitation (>90% to extreme precipitation) across BCSAK (Table 1), ARs play a key role in replenishing freshwater resources of this region. As a result, it is important to investigate the temporal change in the contribution of ARs to precipitation and its extremes over time. Moreover, the patterns in the historical change signal how the contribution of ARs to precipitation may evolve in a future, warmer climate anticipated in this region.

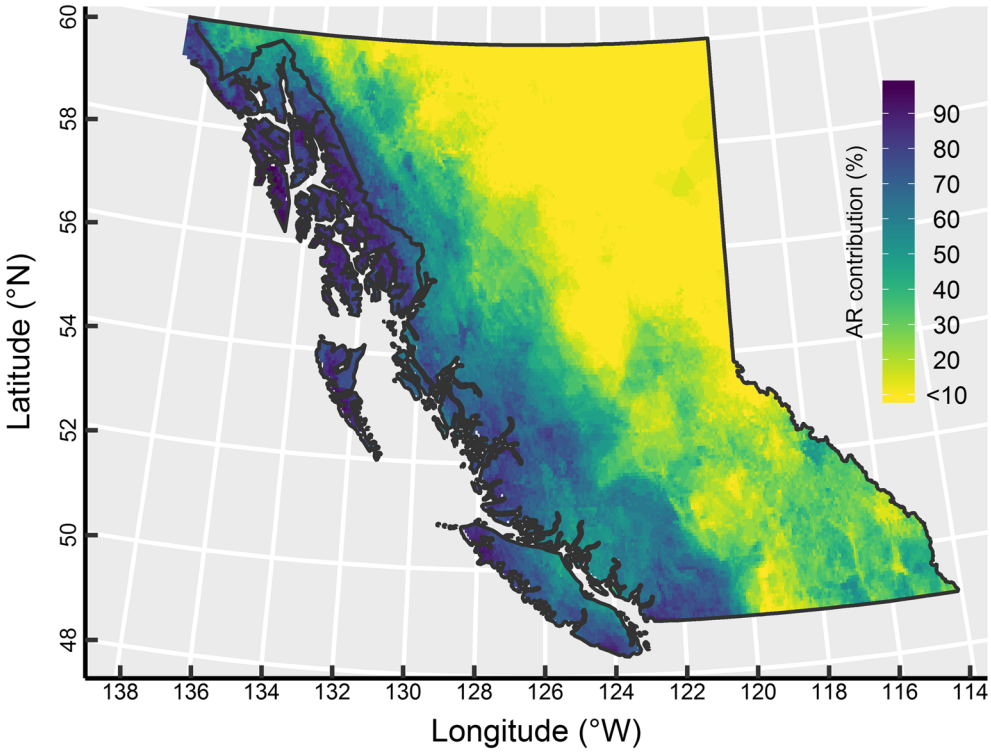

Figure 4. The BCSAK 1979–2012 average contribution of ARs to annual extreme precipitation (%).

The zero-inflated beta regression model coefficients, especially the parameters μ (the mean contribution) and ν (probability of observing zero AR contribution), provide change on AR contributions to precipitation over time. The μ parameter shows no change for most of BCSAK during 1979–2012, except for a small section of north-central BC where the contribution of ARs to precipitation is increasing annually, during autumn and summer (Figures 9 and S6). The parameter σ (variance) indicates decreasing variability in the contribution of ARs to total annual precipitation, especially along the lower latitude regions of BCSAK. The widespread decrease in the ν parameter translates to an increase in the nonzero fractional contribution of ARs to annual and seasonal total (especially autumn and winter) precipitation across most of BCSAK during 1979–2012 (Figures 9 and S6).

The contribution of ARs to extreme precipitation does not show widespread changes across BCSAK during 1979–2012 (Figures S7a and S8). Patches of significant decreases (p value <0.05) occur along Haida Gwaii, northwestern BC, and parts of southeastern BC; few grid points in the Central Interior show a significant increase. However, further evaluation on the field significance of the trend results across BCSAK shows no change over time in both the annual and seasonal contribution of ARs to extreme precipitation.

The temporal dependence of the contribution of ARs to snowfall shows a decreasing pattern along the coastal mountainous region of BCSAK; however, the rate of decrease is not significant (p value >0.05) for most of these grid cells (Figure S7b). Although no significant changes in the contribution of ARs to extreme snowfall occurs for most of BCSAK, some higher elevation grid cells along the Coast Mountains show a significant decrease over 1979–2012 (Figure S9).

4.7. Role of PDO and ENSO on the Contribution of ARs to Precipitation

Most of BCSAK, especially the coastal region, experiences a higher percentage of AR-related winter precipitation during the warm phase of the PDO than the cool phase with a difference of up to 8% (spatial range: −4% to +8%) (Figure 10). The difference is relatively low (spatial range: −3% to +3%) for annual contributions with a slight increase during the warm phase of the PDO than the cool phase, primarily along coastal BCSAK (Figure 10). Moreover, a northward shift in the contribution of ARs to winter precipitation emerges,

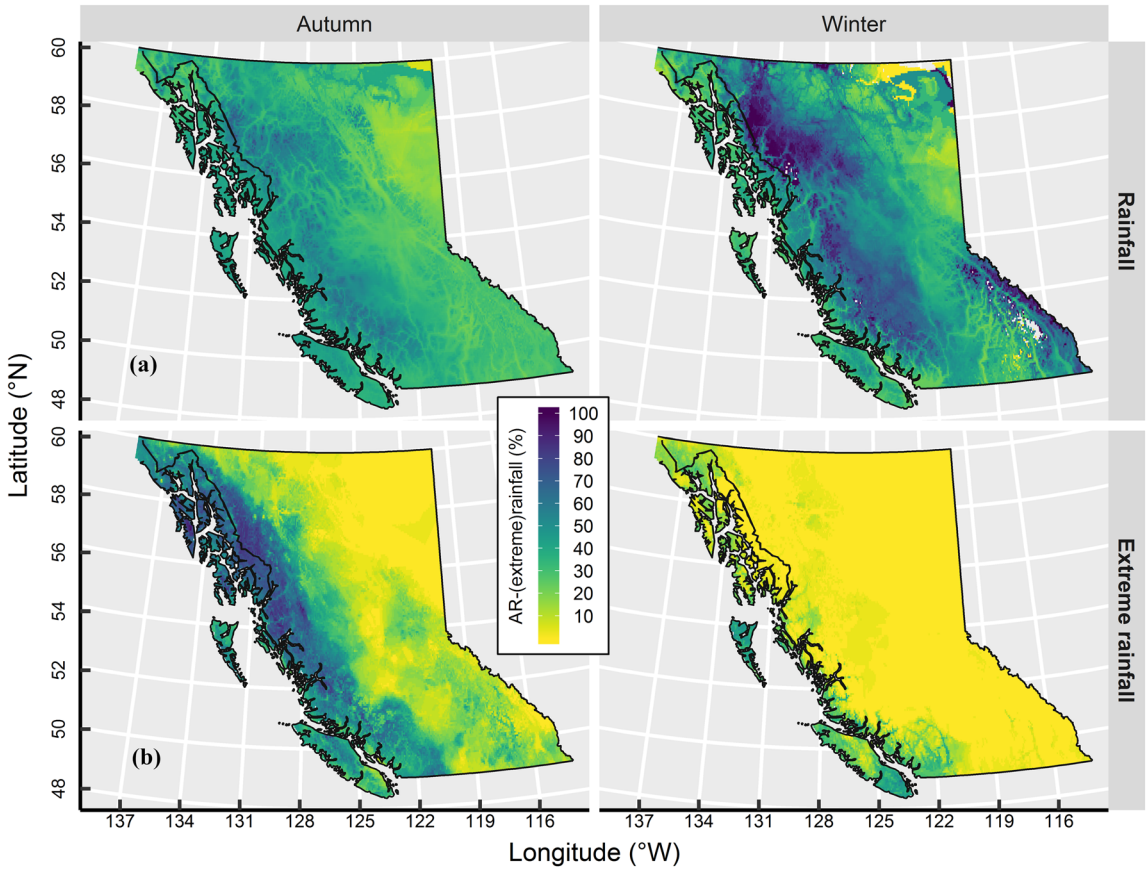

Figure 5. Seasonal (autumn and winter) contribution of ARs to (a) rainfall (percent of total rainfall) and (b) extreme rainfall (percent of total extreme rainfall).

with north-central BC experiencing greater contributions during the positive PDO phase while in southern BC larger amounts occur during the negative PDO phase.

The distribution of the annual and winter season contribution of ARs to the precipitation shows a higher percentage of influence during the neutral phase of ENSO followed by El Niño and La Niña phases, respectively (Figure 11); however, this distribution is not statistically significant (p value >0.05).

5. Discussion

5.1. Comparison With Other Studies

To our knowledge, this study represents the first attempt to quantify AR impacts on precipitation amounts across BCSAK; therefore, results herein are compared with the bordering regions of the Pacific Northwest in the United States. Unlike the western United States and Europe where the contribution of ARs to precipitation attains a maximum (minimum) in winter (summer) (Lavers & Villarini, 2015), BCSAK experiences the highest (lowest) contribution during autumn (spring).

Utilizing gridded precipitation data for 1979–2012, Lavers and Villarini (2015) define AR-related precipitation in each grid cell if its precipitation lies within a 1.5° Euclidian distance from an AR axis and report ~30% contribution of ARs to the average monthly precipitation along the coast of Washington and Oregon (WAOR). Results herein observed on the western arc of the Coast Mountains of BCSAK including Vancouver Island, Haida Gwaii, and southeastern AK (Figure 2a) are generally consistent with Lavers and Villarini (2015). Discrepancies arise however in seasonal values; for example, ARs provide higher monthly contributions in coastal BCSAK (up to ~55% in September/October) compared to the coastal region of WAOR (up to ~40% in October/November). These variations arise likely due to the higher frequency of landfalling ARs in BCSAK compared to WAOR, especially during early autumn (Gershunov et al., 2017;

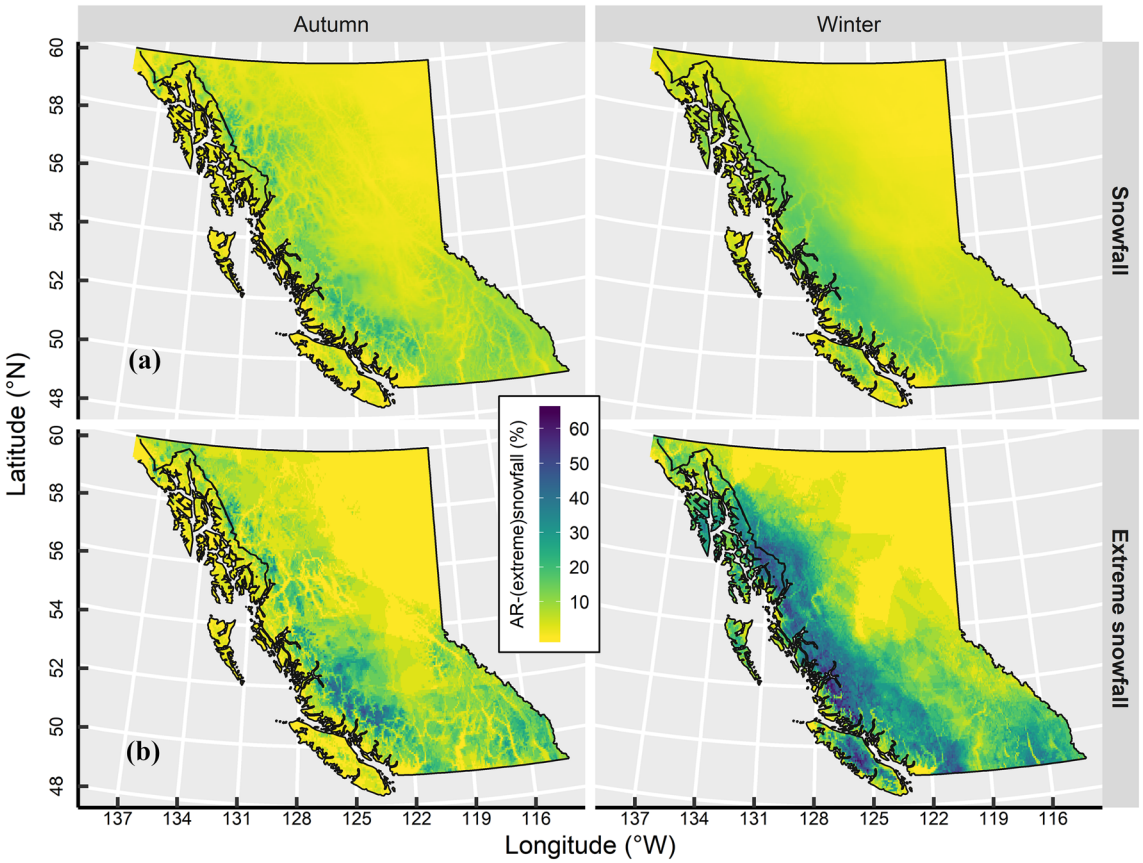

Figure 6. Seasonal (autumn and winter) contribution of ARs to (a) snowfall (percent of total snowfall) and (b) extreme snowfall (percent of total extreme snowfall).

Sharma & Déry, 2020) and/or the difference in the definition of AR-related precipitation. Findings from this research are consistent with many recent studies that have analyzed the contribution of ARs to the total and extreme precipitation along coastal areas exposed to westerly maritime flows where the impacts of ARs are known to be substantial (Dettinger et al., 2011; Guan et al., 2010; Lavers & Villarini, 2013, 2015; Rutz & Steenburgh, 2012; Viale et al., 2018). A comparison of the contribution of ARs to monthly precipitation shows that coastal regions of BCSAK experience higher AR contributions in a single month (up to 57% in September) compared to the West Coast of the United States (up to 40% in November) (Lavers & Villarini, 2015). However, BCSAK receives less AR-related total annual precipitation than the amount observed in lower latitudinal regions of western North America (e.g., California; Gershunov et al., 2017), southern South America (Viale et al., 2018), and the Iberian Peninsula (Lavers & Villarini, 2015).

ARs act as a key, and in some cases, the only meteorological factor responsible for extreme precipitation in BCSAK with an annual contribution up to 97% (100% during autumn) in some coastal areas (Figure 4). Findings here generally agree with previous studies that report a substantial contribution of ARs to extreme precipitation along coastal basins globally. For example, Lamjiri et al. (2017) report 60%–100% of the 1948–2002 extreme events, defined as storms with precipitation total return intervals >2 years over the West Coast of the United States, arise from ARs. In Western Europe, Lavers and Villarini (2013), using annual maxima daily precipitation (similar to the approach used in this study) over 1979–2011, find up to 80% of the 10 largest daily rainfall events are associated with ARs. Azad and Sorteberg (2017) report 94% linkages between ARs and extreme daily precipitation events defined as precipitation >99.5% percentile in coastal Norway, and Viale et al. (2018) show 50–70% of the most intense rainy days are linked to ARs in southwestern South America. Results in this paper compare favorably to the aforementioned studies and confirm ARs act as key causative factor for extreme precipitation along coastal basins globally including BCSAK.

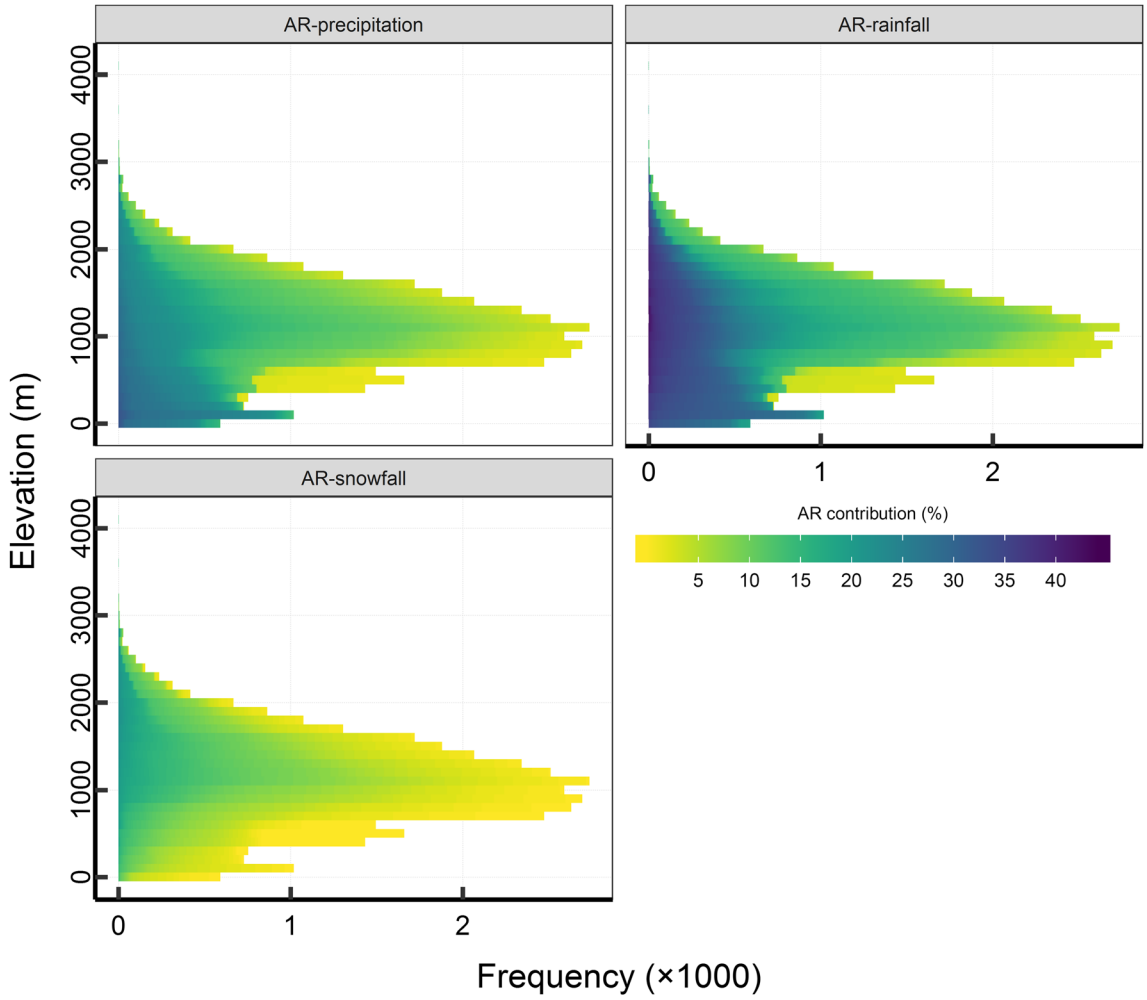

Figure 7. Elevational distribution of the percentage of AR-related annual precipitation, rainfall, and snowfall at different elevation ranges (bin sizes of 100 m) of BCSAK during 1979–2012. The color gradient represents the percentage of AR contribution on each grid cell across BCSAK.

5.2. AR-Related Precipitation During the PDO and ENSO

Previous studies report higher amounts of precipitation across BCSAK during the cool (negative) phase of the PDO and the La Niña phase of the ENSO (Fleming & Whitfield, 2010; Shabbar et al., 1997). Higher AR-related precipitation is observed in BCSAK during the same phases of the PDO and ENSO when more ARs make landfall (Sharma & Déry, 2020). Dettinger (2004) and Spry et al. (2014) report similar findings as that of this study when they evaluated the amount of precipitation associated with Pineapple Expresses during the phases of the PDO and ENSO for the western United States and the lower mainland of BC, respectively. Moreover, Dettinger et al. (2011) observed >50% positive correlation between AR-related precipitation and the positive phase of the PDO along western Washington; the correlation was positive but weaker with the Nino3.4 index in the same region. The southward displacement of the climatological Aleutian Low pressure pattern during the neutral phase of ENSO and positive phase of the PDO provides the westerlies greater access to warm tropical moisture (Dettinger et al., 2011; Mantua et al., 1997; Spry et al., 2014) and thus leading to greater amounts of precipitation. Precipitation amounts during AR-days are greater relative to other (non-AR) precipitation days (Dettinger, 2004; Guan et al., 2010), leading to substantially higher precipitation even with a small increase in AR frequency. Of note, ocean-atmosphere variability such as the PDO and ENSO influences the seasonal precipitation anomalies following some lag and may not directly influence extreme precipitation events of shorter duration associated with ARs (Fleming & Whitfield, 2010; Spry et al., 2014).

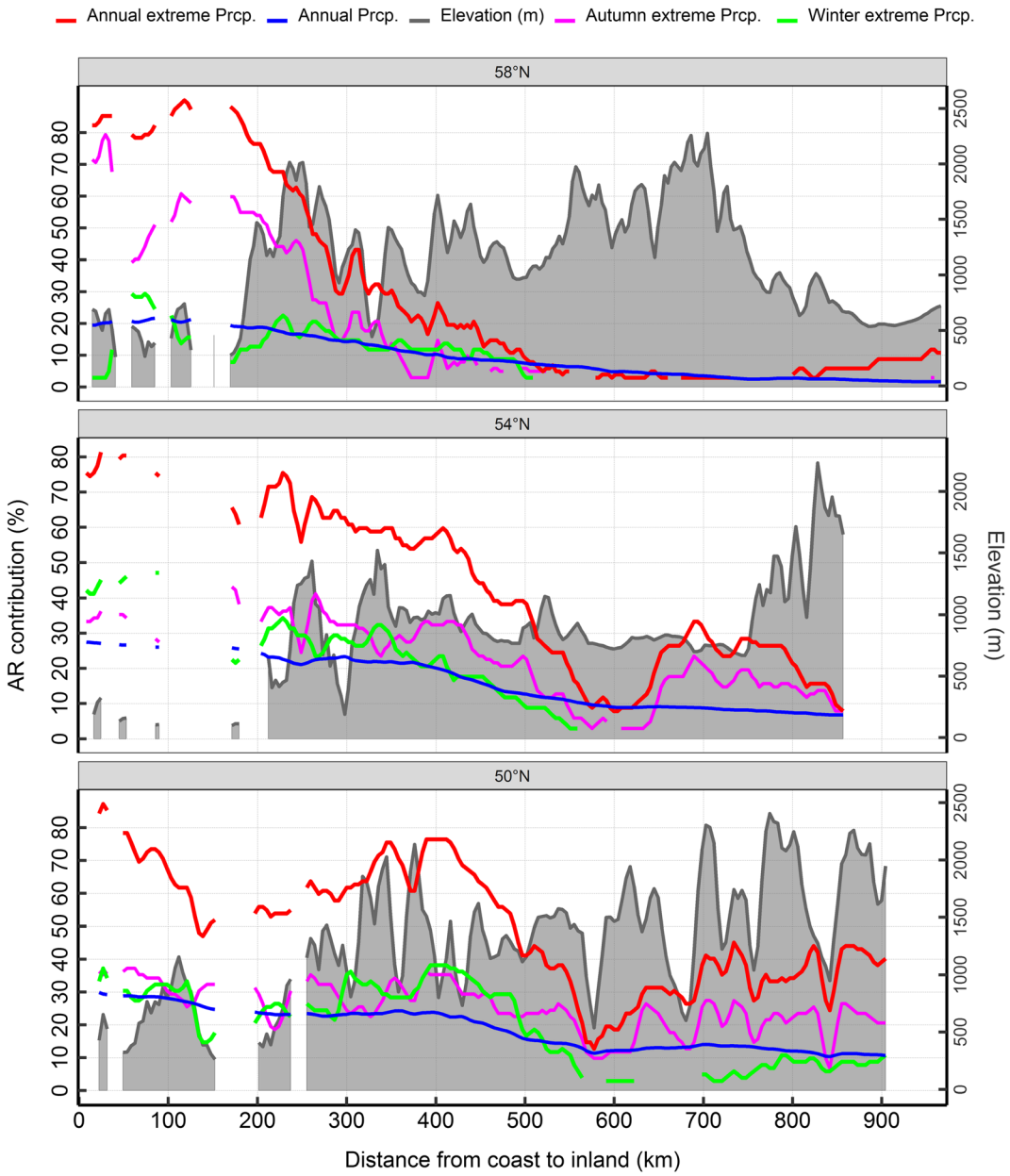

Figure 8. Profiles of the elevational dependence and the contribution of ARs to precipitation and its extremes inland along the transects near the 50°N, 54°N, and 58°N parallels across BCSAK during 1979–2012. Curves denote three-point running averages of a given quantity, while breaks along the transects show the transition from islands to the mainland (see Figure 1a).

5.3. Changes in AR Contribution Over Time and Future Projections

The decrease in the parameter ν (nonzero probability of the contribution of ARs to precipitation) arises likely due to an increase in the frequency of landfalling ARs along coastal BCSAK during 1979–2016 (Sharma & Déry, 2020) and is linked to AR variations caused by the northward shift of Pacific storm tracks (Chang & Yau, 2016; Salathé, 2006), and/or changes in atmospheric moisture content (Santer et al., 2007; Sharma & Déry, 2020; Wentz et al., 2007). Although a significant decrease occurs in parameter ν (probability of observing zero contribution of ARs to precipitation), parameter μ (mean AR contribution to precipitation) does not exhibit such an increase for most of BCSAK perhaps due to an overall increase in the total precipitation, including the precipitation associated with convective activity in response to an increase in surface air temperatures (Berg et al., 2013; Vincent et al., 2015; Wentz et al., 2007; Zhang

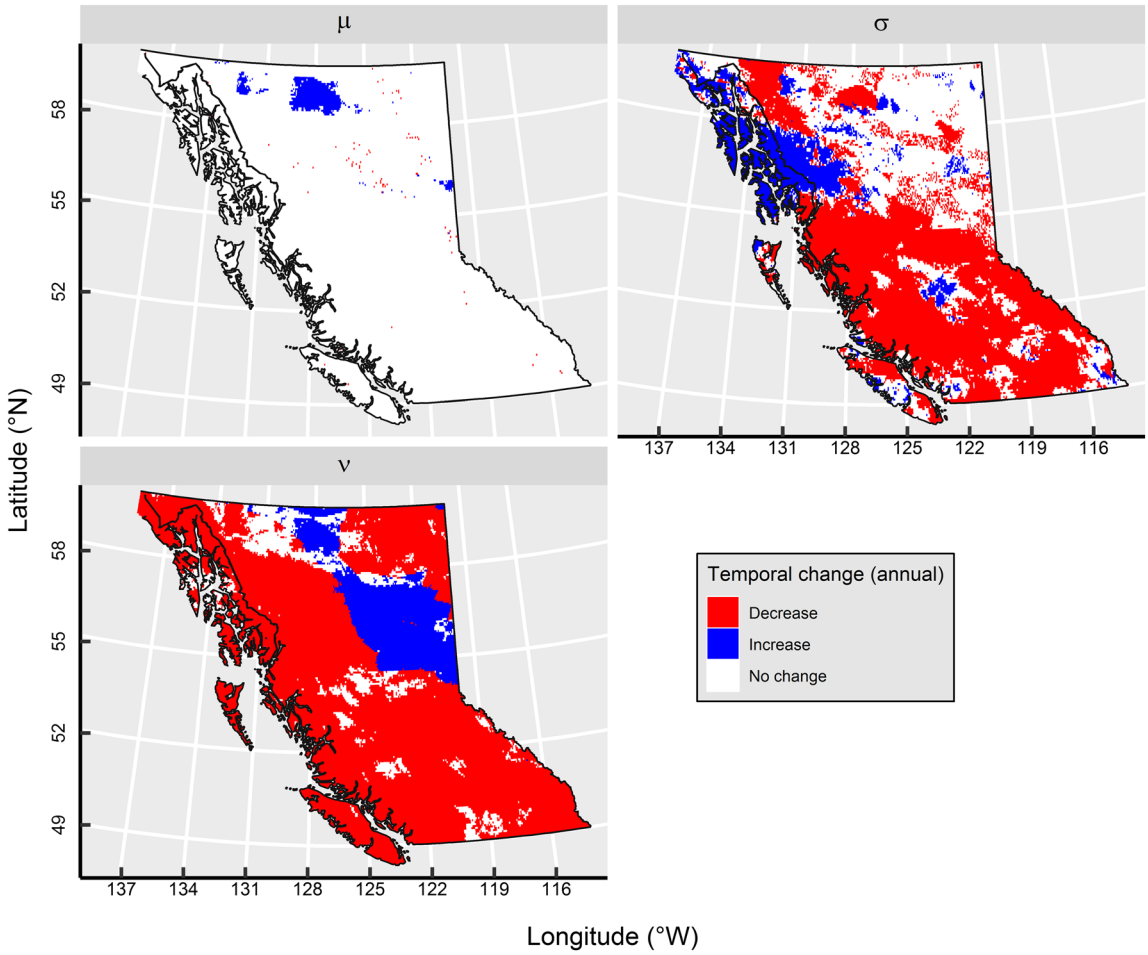

Figure 9. Maps of BCSAK showing temporal changes (directional) in the average annual contribution of ARs to precipitation given by the change on the parameters μ (mean AR contribution to precipitation), σ (variance in the contribution of ARs to precipitation), and ν (probability of observing zero contribution of ARs to precipitation) of the zero-inflated beta regression, 1979–2012.

et al., 2000). Moreover, rises in the surface air temperature, especially in recent decades, lead to increases in atmospheric water vapor content in-line with the Clausius-Clapeyron equation (Dessler et al., 2008; Tsonis, 2013). This causes the IVT to be higher, inducing more frequent exceedances of its threshold of 250 kg m^{-1} s^{-1} to define the AR-related precipitation. In turn, this leads to increases in the nonzero probability of the contribution of ARs to precipitation. The patterns observed in the changes on the historical contribution of ARs to precipitation align with model-based future projections. For example, Warner et al. (2015) and Radić et al. (2015) project increased frequency of ARs along the North American West Coast and BCSAK by 2100 and 2070–2100, respectively. This will lead to an increase in the number of days with AR-related precipitation; a pattern also observed in the historical contribution as shown by changes in parameter ν (nonzero probability of the contribution of ARs to precipitation).

The decrease in the contribution of ARs to snowfall and its extremes observed in some of the higher elevation grid cells along the coastal mountainous region of BCSAK is likely associated with warming trends of landfalling ARs in recent decades. Gonzales et al. (2019) find that the cold season ARs landfalling along the West Coast of the United States have warmed (range of warming 0.69 to 1.65 °C) during 1980–2016 owing to the combined influence of regional and oceanic warming. Similar signals of warmer ARs occurring in northern latitudes are likely resulting in a decrease in the contribution of ARs to snowfall along the mountainous regions of BCSAK (Sharma & Déry, 2020). The decreasing pattern of the contribution of ARs to snowfall has important consequences on water storage and river runoff of BCSAK.

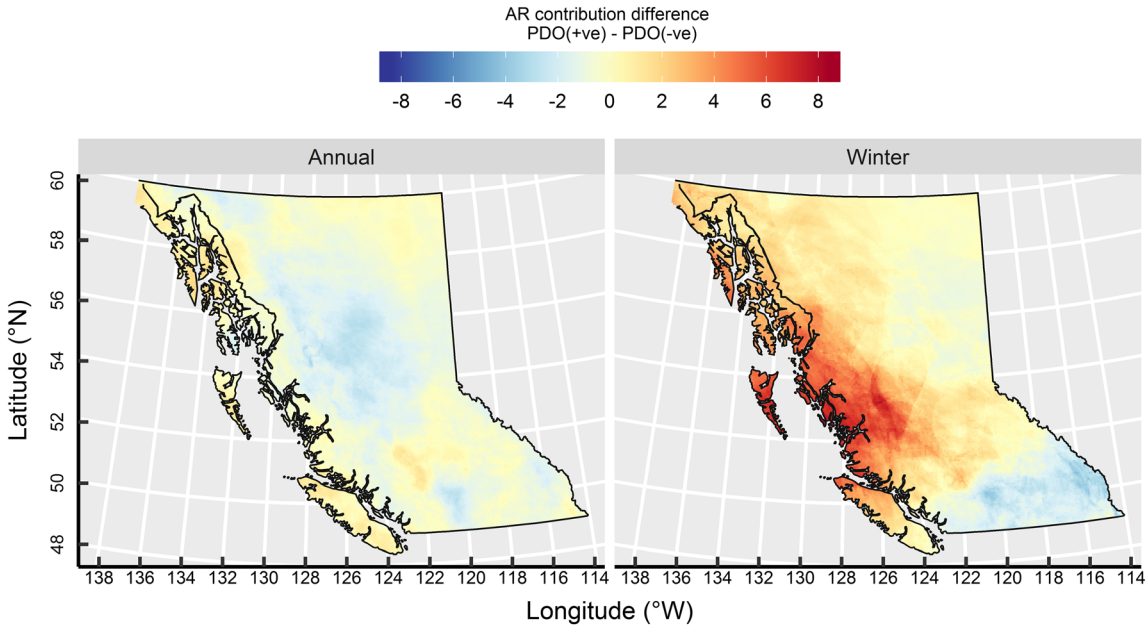

Figure 10. The difference in the percentage of the contribution of ARs to precipitation between the warm (1977–1999) and cool (1948–1976) phases of the PDO for annual and winter.

5.4. Study Limitations and Uncertainties

Results on the AR contribution to precipitation and its extremes are susceptible to four primary sources of uncertainty, as follows: (i) the biases of PNWNAmet gridded precipitation data as discussed in sub section 3.1.1, (ii) the AR-detection algorithm and resolution of the reanalysis data, (iii) the IVT threshold ($\geq$250 kg m^{-1} s^{-1}) that characterizes ARs, and (iv) the methodological limitation associated with the block maxima approach, which is restricted by the relatively short period of study.

Differences in AR-detection algorithms, reanalysis data assimilation, and their resolution create disparate AR chronologies and IVT fields (Rutz et al., 2019). Therefore, we perform a sensitivity analysis to explore differences in AR-related precipitation between the relatively coarse resolution (2.5° × 2.5°) NCEP/NCAR-based IVT fields used in this study and the relatively high resolution (0.625° longitude × 0.5° latitude) IVT fields calculated using specific humidity and wind fields from Modern-Era Retrospective Analysis for Research and Applications (MERRA2; Gelaro et al., 2017) data. The spatially averaged annual AR contribution to precipitation is nearly identical between MERRA2 (12.1 ± 10%) and NCEP/NCAR (12.7 ± 8%); however, the contribution of ARs to extreme precipitation is slightly higher in the NCEP/NCAR (35 ± 26%) than the MERRA2 (32 ± 28%) across BCSAK, 1982–2012. The slightly higher spatially averaged mean from NCEP/NCAR compared to MERRA2 is perhaps due to the topographic complexities in BCSAK. The percentage of AR contribution from low-resolution NCEP/NCAR data is smoother across larger areas of BCSAK than MERRA2, a feature that is also illustrated by a wider range of contribution percentage from MERRA2 (0%–40%) than NCEP/NCAR (1%–32%) (Figure S10). Furthermore, the spatial distribution of average contribution of ARs to precipitation based on MERRA2 IVT exceeds that of NCEP/NCAR along the coastal regions of BCSAK. However, the MERRA2 results show lower AR contributions in the interior mountainous regions (e.g., along the Rocky and Columbia Mountains) (Figure S11). Apart from NCEP/NCAR and MERRA2 comparisons, an expansion of our analyses with multiple reanalyses and climate model simulations would improve the robustness of the results.

The use of a fixed higher (lower) IVT threshold may decrease (increase) the AR contribution percentage to precipitation. For example, the average AR contribution to precipitation across BCSAK is 11 ± 8% when considering an IVT threshold of $\geq$350 kg m^{-1} s^{-1} whereas that with IVT threshold of $\geq$250 kg m^{-1} s^{-1} is 13 ± 7% indicating a relatively minor difference in the AR contribution with the change in IVT of 100 kg m^{-1} s^{-1}. Moreover, grid cell precipitation matching the IVT threshold was considered as AR related; however,

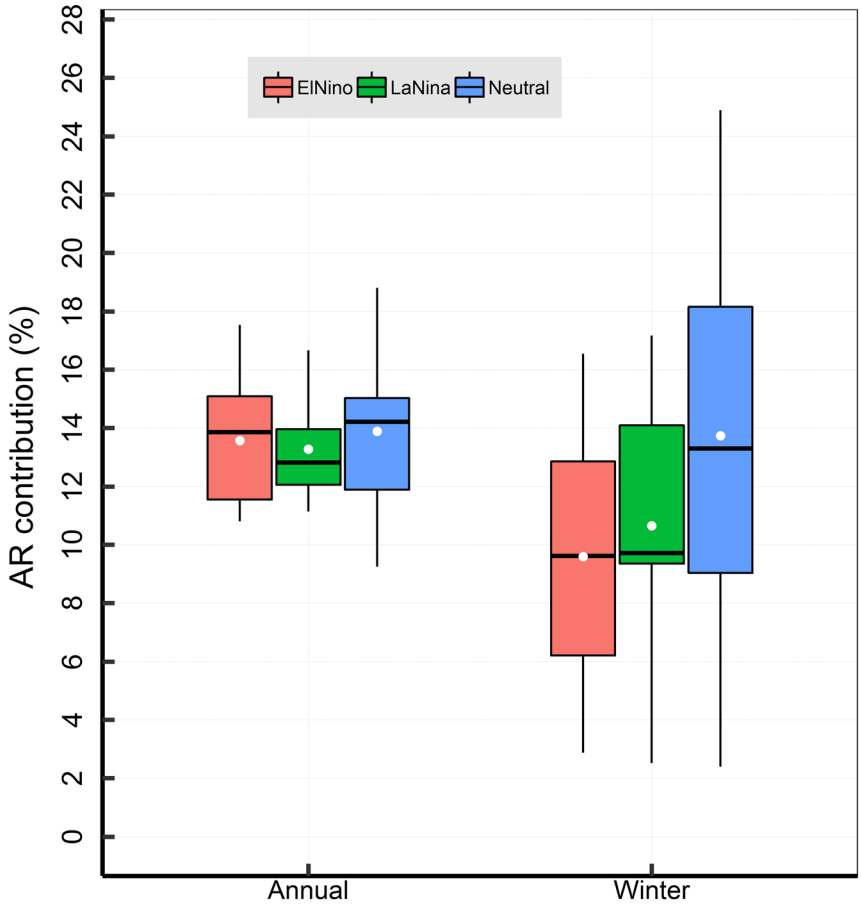

Figure 11. Box and whiskers plots showing the distribution of the contribution of ARs to precipitation during different phases of ENSO (El Niño 10 years, La Niña 6 years, and neutral 18 years), 1979–2012 across BCSAK. The black horizontal lines indicate the median, the white dots show the mean, and the vertical black lines indicate the range of percentage of contribution within 1.5 the interquartile range.

precipitation (if any) in adjacent grid cells that does not satisfy the IVT threshold was not considered as AR related. Besides, the generalization of this study's results on the contribution of ARs to extreme precipitation represents only a subset of these events (34 annual and 4 × 34 seasonal; obtained through an implementation of the block maxima approach [see section 3.2.1]) and does not include linkages between all extreme precipitation events and ARs across BCSAK. Despite these limitations and uncertainties, this effort provides much needed quantitative results on the contribution of ARs to rainfall, snowfall, and their extremes over an area that is otherwise poorly studied while providing direction for future work.

6. Conclusions

The objective of this study was to quantify the contribution of ARs to precipitation (including its partitioning into rainfall and snowfall) and its extremes across BCSAK during 1979–2012. Using a newly developed, high-resolution gridded precipitation data set, and the NCEP/NCAR reanalysis-based AR catalog and IVT, we assessed the percentage of annual, seasonal, and extreme precipitation associated with ARs in BCSAK, parts of which are some of the wettest locations on Earth. Results suggest that ARs play a key role in transporting the (sub)tropical moisture from the Pacific Ocean to BCSAK and often acting as a causative factor for extreme precipitation events, particularly along coastal and mountainous regions.

The contribution of ARs to average total annual precipitation ranges from >33% along the coastal region of BCSAK to <5% in northeastern BC. Strong seasonality exists in the average AR contribution to precipitation with the highest amount during autumn (~21%), and the lowest in spring (~3%). The contribution of ARs to

precipitation decreases rapidly from the coastal region of BCSAK to the lee of the Coast Mountains and then more gradually across the Interior Plateau. ARs act as the main synoptic-scale mechanism that leads to rainfall in the Columbia and Rocky Mountains in winter, perhaps leading to rain-on-snow events in winter and early spring. An examination of the temporal change of AR contribution to precipitation using a zero-inflated beta regression model reveals an increase in the nonzero contribution but no change on the average contribution for most of BCSAK during 1979–2012. In BCSAK, ARs act as a substantial causative factor for extreme precipitation, with >90% contribution, especially across mountainous regions likely due to orographically enhanced precipitation. The contribution of ARs to precipitation depends on the frequency of landfalling ARs and orographic characteristics; therefore, factors that impact landfalling AR frequency also affect the contribution of ARs to precipitation in BCSAK.

Results herein reinforce the key role ARs play in transporting water vapor to northern midlatitude regions of western North America from the (sub)tropical basins of the Pacific Ocean. In addition, it augments knowledge on AR-associated precipitation that influences rainfall, snowfall, and hence snowpack and glacier processes, which largely govern the hydroclimatology of this region. Future work will focus on investigations of river discharge and the hydrological response to ARs across BCSAK, and an examination of how ARs modulate mountain snowpacks in this region. This work improves the quantitative understanding that ARs constitute a critical role in the precipitation of BCSAK. An improved understanding of quantitative precipitation in BCSAK has broader implications on community water supply and management, hydropower operations, flood mitigation, and ecological and recreational water values.

Acknowledgments
Thanks to Markus Schnorbus (PCIC) and Alex Cannon (ECCC) for providing the PNWNAmet data set and the creators and contributors of the SIO-R1-catalog. Thanks to Brian Menounos (UNBC), Ellen Petticrew (UNBC), Alex Cannon (ECCC), and John Gyakum (McGill University) for their suggestions on the manuscript. Thanks to Hadleigh Thompson (UQAM) and Jeremy Morris (UNBC) for proofreading an earlier draft of the manuscript. Funding provided by UNBC, the Nechako Environmental Enhancement Fund (NEEF), the Real Estate Foundation of BC, and the Mountain Water Futures project of the Global Water Futures (GWF) programme. Thanks to three anonymous referees who provided constructive comments on this work that led to a much improved paper. All data sets used in this paper are publicly available through the references cited and can be accessed through the web portals https://www.pacificclimate.org/data/daily-gridded-meteorological-datasets (PNWNAmet precipitation and temperature data) and http://cw3e.ucsd.edu/Publications/SIO-R1-Catalog/ (SIO-R1 AR catalog data).

References

Akaike, H. (1974). A new look at the statistical model identification. *IEEE Transactions on Automatic Control*, *19*(6), 716–723. https://doi.org/10.1109/TAC.1974.1100705

Azad, R., & Sorteberg, A. (2017). Extreme daily precipitation in coastal western Norway and the link to atmospheric rivers. *Journal of Geophysical Research-Atmospheres*, *122*, 2080–2095. https://doi.org/10.1002/2016JD025615

Bao, J. W., Michelson, S. A., Neiman, P. J., Ralph, F. M., & Wilczak, J. M. (2006). Interpretation of enhanced integrated water vapor bands associated with extratropical cyclones: Their formation and connection to tropical moisture. *Monthly Weather Review*, *134*(4), 1063–1080. https://doi.org/10.1175/MWR3123.1

Berg, P., Moseley, C., & Haerter, J. O. (2013). Strong increase in convective precipitation in response to higher temperatures. *Nature Geoscience*, *6*(3), 181–185. https://doi.org/10.1038/ngeo1731

Blanchet, J., Marty, C., & Lehning, M. (2009). Extreme value statistics of snowfall in the Swiss Alpine region. *Water Resources Research*, *45*, W05424. https://doi.org/10.1029/2009WR007916

Chang, E. K. M., & Yau, A. M. W. (2016). Northern Hemisphere winter storm track trends since 1959 derived from multiple reanalysis datasets. *Climate Dynamics*, *47*(5–6), 1435–1454. https://doi.org/10.1007/s00382-015-2911-8

Chen, X., Leung, L. R., Gao, Y., Liu, Y., Wigmosta, M., & Richmond, M. (2018). Predictability of extreme precipitation in western U.S. watersheds based on atmospheric river occurrence, intensity, and duration. *Geophysical Research Letters*, *45*(11), 693–11,701. https://doi.org/10.1029/2018GL079831

Church, M., & Ryder, J. (2010). Physiography of British Columbia. In R. Pike, T. E. Redding, R. D. Moore, R. D. Winkler, & K. D. Bladon (Eds.), *Compendium of forest hydrology and geomorphology in British Columbia*. B.C. Min. For. Range, For. Sci. Prog., Victoria, B.C. and FORREX Forum for Research and Extension in Natural Resources, Kamloops, B.C. Land Manag. Handb. 66. Retrieved from https://www.for.gov.bc.ca/hfd/pubs/Docs/Lmh/Lmh66.htm

Coles, S. (2001). *An introduction to statistical modeling of extreme values*. London: Springer. https://doi.org/10.1007/978-1-4471-3675-0

Curry, C. L., Islam, S. u., Zwiers, F. W., & Déry, S. J. (2019). Atmospheric rivers increase future flood risk in Western Canada's largest Pacific River. *Geophysical Research Letters*, *46*, 1651–1661. https://doi.org/10.1029/2018GL080720

Dessler, A. E., Zhang, Z., & Yang, P. (2008). Water-vapor climate feedback inferred from climate fluctuations, 2003-2008. *Geophysical Research Letters*, *35*(20), L20704. https://doi.org/10.1029/2008GL035333

Dettinger, M. D. (2004). Fifty-two years of "pineapple-express" storms across the West Coast of North America. US Geological Survey, Scripps Institution of Oceanography for the California Energy Commission,PIER Energy-Related Environmental Research. CEC-500-2005-004.

Dettinger, M. D., Ralph, F. M., Das, T., Neiman, P. J., & Cayan, D. R. (2011). Atmospheric rivers, floods and the water resources of California. *Water*, *3*(2), 445–478. https://doi.org/10.3390/w3020445

Fahrmeir, L., Kneib, T., Lang, S., & Marx, B. (2013). *Regression models, Methods and Applications*. London: Springer. https://doi.org/10.1007/978-3-642-34333-9

Ferrari, S. L. P., & Cribari-Neto, F. (2004). Beta regression for modelling rates and proportions. *Journal of Applied Statistics*, *31*(7), 799–815. https://doi.org/10.1080/0266476042000214501

Fleming, S. W., & Whitfield, P. H. (2010). Spatiotemporal mapping of ENSO and PDO surface meteorological signals in British Columbia, Yukon, and Southeast Alaska. *Atmosphere-Ocean*, *48*(2), 122–131. https://doi.org/10.3137/AO1107.2010

Gelaro, R., McCarty, W., Suárez, M. J., Todling, R., Molod, A., Takacs, L., et al. (2017). The modern-era retrospective analysis for research and applications, version 2 (MERRA-2). *Journal of Climate*, *30*(13), 5419–5454. https://doi.org/10.1175/JCLI-D-16-0758.1

Gershunov, A., Shulgina, T., Ralph, F. M., Lavers, D. A., & Rutz, J. J. (2017). Assessing the climate-scale variability of atmospheric rivers affecting western North America. *Geophysical Research Letters*, *44*(15), 7900–7908. https://doi.org/10.1002/2017GL074175

Gimeno, L., Stohl, A., Trigo, R. M., Dominguez, F., Yoshimura, K., Yu, L., et al. (2012). Oceanic and terrestrial sources of continental precipitation. *Reviews of Geophysics*, *50*(4), RG4003. https://doi.org/10.1029/2012RG000389

Goldenson, N., Leung, L. R., Bitz, C. M., & Blanchard-Wrigglesworth, E. (2018). Influence of atmospheric rivers on mountain snowpack in the Western United States. *Journal of Climate*, *31*, 9921–9940. https://doi.org/10.1175/JCLI-D-18-0268.1

Gonzales, K. R., Swain, D. L., Nardi, K. M., Barnes, E. A., & Diffenbaugh, N. S. (2019). Recent warming of landfalling atmospheric rivers along the west coast of the United States. *Journal of Geophysical Research-Atmospheres*, *124*(13), 6810–6826. https://doi.org/10.1029/2018JD029860

Gorodetskaya, I. V., Tsukernik, M., Claes, K., Ralph, F. M., Neff, W. D., & Lipzig, N. P. M. V. (2014). The role of atmospheric rivers in anomalous snow accumulation in East Antarctica. *Geophysical Research Letters*, *41*, 6199–6206. https://doi.org/10.1002/2014GL060881

Guan, B., Molotch, N. P., Waliser, D. E., Fetzer, E. J., & Neiman, P. J. (2010). Extreme snowfall events linked to atmospheric rivers and surface air temperature via satellite measurements. *Geophysical Research Letters*, *37*, L20401. https://doi.org/10.1029/2010GL044696

Guan, B., & Waliser, D. E. (2015). Detection of atmospheric rivers: Evaluation and application of an algorithm for global studies. *Journal of Geophysical Research-Atmospheres*, *120*(12), 12,514–12,535. https://doi.org/10.1002/2015JD024257

Hare, F. K. (1998). Canada's climate: An overall perspective. In W. G. Bailey, T. R. Oke, & W. R. Rouse (Eds.), *The surface climates of Canada* (pp. 3–20). Montreal: McGill-Queen's University Press.

Hawcroft, M. K., Shaffrey, L. C., Hodges, K. I., & Dacre, H. F. (2012). How much northern hemisphere precipitation is associated with extratropical cyclones? *Geophysical Research Letters*, *39*(24), L24809. https://doi.org/10.1029/2012GL053866

Hernández-Henríquez, M. A., Sharma, A. R., & Déry, S. J. (2017). Variability and trends in runoff in the rivers of British Columbia's Coast and Insular Mountains. *Hydrological Processes*, *31*(18), 3269–3282. https://doi.org/10.1002/hyp.11257

Holland, S. S. (1976). Landforms of British Columbia: A physiographic outline. British Columbia Department of Mines and Petroleum Resources, Bulletin No. 48.

Hollander, M., Wolfe, D. A., & Chicken, E. (2014). *Nonparametric statistical methods*, (3rd ed.). New York: John Wiley & Sons.

Jain, S. K., Kumar, V., & Saharia, M. (2013). Analysis of rainfall and temperature trends in northeast India. *International Journal of Climatology*, *33*, 968–978. https://doi.org/10.1002/joc.3483

Kalnay, E., Kanamitsu, M., Kistler, R., Collins, W., Deaven, D., Gandin, L., ... Joseph, D. (1996). The NCEP/NCAR 40-year reanalysis project. *Bulletin of the American Meteorological Society*, *77*(3), 437–471. https://doi.org/10.1175/1520-0477(1996)077<0437:TNYRP>2.0.CO;2

Kienzle, S. W. (2008). A new temperature based method to separate rain and snow. *Hydrological Processes*, *22*, 5067–5085. https://doi.org/10.1002/hyp.7131

Konrad, C. P., & Dettinger, M. D. (2017). Flood runoff in relation to water vapor transport by atmospheric rivers over the western United States, 1949–2015. *Geophysical Research Letters*, *44*, 11,456–11,462. https://doi.org/10.1002/2017GL075399

Lamjiri, M. A., Dettinger, M. D., Ralph, F. M., & Guan, B. (2017). Hourly storm characteristics along the U.S. west coast: Role of atmospheric rivers in extreme precipitation. *Geophysical Research Letters*, *44*, 7020–7028. https://doi.org/10.1002/2017GL074193

Lavers, D. A., Allan, R. P., Villarini, G., Lloyd-Hughes, B., Brayshaw, D. J., & Wade, A. J. (2013). Future changes in atmospheric rivers and their implications for winter flooding in Britain. *Environmental Research Letters*, *8*(3), 034010. https://doi.org/10.1088/1748-9326/8/3/034010

Lavers, D. A., Allan, R. P., Wood, E. F., Villarini, G., Brayshaw, D. J., & Wade, A. J. (2011). Winter floods in Britain are connected to atmospheric rivers. *Geophysical Research Letters*, *38*, L23803. https://doi.org/10.1029/2011GL049783

Lavers, D. A., Ralph, F. M., Waliser, D. E., Gershunov, A., & Dettinger, M. D. (2015). Climate change intensification of horizontal water vapor transport in CMIP5. *Geophysical Research Letters*, *42*, 5617–5625. https://doi.org/10.1002/2015GL064672

Lavers, D. A., & Villarini, G. (2013). The nexus between atmospheric rivers and extreme precipitation across Europe. *Geophysical Research Letters*, *40*(12), 3259–3264. https://doi.org/10.1002/grl.50636

Lavers, D. A., & Villarini, G. (2015). The contribution of atmospheric rivers to precipitation in Europe and the United States. *Journal of Hydrology*, *522*, 382–390. https://doi.org/10.1016/j.jhydrol.2014.12.010

Lavers, D. A., Villarini, G., Allan, R. P., Wood, E. F., & Wade, A. J. (2012). The detection of atmospheric rivers in atmospheric reanalyses and their links to British winter floods and the large-scale climatic circulation. *Journal of Geophysical Research-Atmospheres*, *117*(D20), D20106. https://doi.org/10.1029/2012JD018027

Lin, Y., Chiao, S., Kaplan, M. L., & Weglarz, R. P. (2001). Some common ingredients for heavy orographic rainfall. *Weather and Forecasting*, *16*, 633–660. https://doi.org/10.1175/1520-0434(2001)016<0633:SCIFHO>2.0.CO;2

Mantua, N. J., & Hare, S. R. (2002). The Pacific decadal oscillation. *Journal of Oceanography*, *58*(1), 35–44. https://doi.org/10.1023/A:1015820616384

Mantua, N. J., Hare, S. R., Zhang, Y., Wallace, J. M., & Francis, R. C. (1997). A Pacific interdecadal climate oscillation with impacts on salmon production. *Bulletin of the American Meteorological Society*, *78*(6), 1069–1079. https://doi.org/10.1175/1520-0477(1997)078<1069:APICOW>2.0.CO;2

McKenney, D. W., Hutchinson, M. F., Papadopol, P., Lawrence, K., Pedlar, J., Campbell, K., et al. (2011). Customized spatial climate models for North America. *Bulletin of the American Meteorological Society*, *92*(12), 1611–1622. https://doi.org/10.1175/2011BAMS3132.1

Meehl, G. A., Hu, A., & Santer, B. D. (2009). The mid-1970s climate shift in the Pacific and the relative roles of forced versus inherent decadal variability. *Journal of Climate*, *22*(3), 780–792. https://doi.org/10.1175/2008JCLI2552.1

Moore, R. D., Spittlehouse, D. L., Whitfield, P. H., & Stahl, K. (2010). Weather and Climate. In K. D. Pike, R.G., Redding, T.E., Moore, R.D., Winkler, R.D. and Bladon (Ed.), *Compendium of forest hydrology and geomorphology in British Columbia*. B.C. Min. For. Range, For. Sci. Prog., Victoria, B.C. and FORREX Forum for Research and Extension in Natural Resources, Kamloops, B.C. Land Manag. Handb. 66. Retrieved from https://www.for.gov.bc.ca/hfd/pubs/Docs/Lmh/Lmh66.htm

Murata, F., Hayashi, T., Matsumoto, J., & Asada, H. (2007). Rainfall on the Meghalaya plateau in northeastern India—One of the rainiest places in the world. *Natural Hazards*, *42*, 391–399. https://doi.org/10.1007/s11069-006-9084-z

Neiman, P. J., Ralph, F. M., White, A. B., Kingsmill, D. E., & Persson, P. O. G. (2002). The statistical relationship between upslope flow and rainfall in California's Coastal Mountains: Observations during CALJET. *Monthly Weather Review*, *130*, 1468–1492. https://doi.org/10.1175/1520-0493(2002)130<1468:TSRBUF>2.0.CO;2

Neiman, P. J., Ralph, F. M., Wick, G. A., Lundquist, J. D., & Dettinger, M. D. (2008). Meteorological characteristics and overland precipitation impacts of atmospheric rivers affecting the west coast of North America based on eight years of SSM/I satellite observations. *Journal of Hydrometeorology*, *9*(1), 22–47. https://doi.org/10.1175/2007JHM855.1

O'Neel, S., Hood, E., Bidlack, A. L., Fleming, S. W., Arimitsu, M. L., Arendt, A., et al. (2015). Icefield-to-ocean linkages across the northern Pacific coastal temperate rainforest ecosystem. *Bioscience*, *65*(5), 499–512. https://doi.org/10.1093/biosci/biv027

Ospina, R., & Ferrari, S. L. P. (2010). Inflated beta distributions. *Statistical Papers*, *51*(1), 111–126. https://doi.org/10.1007/s00362-008-0125-4

Ospina, R., & Ferrari, S. L. P. (2012). A general class of zero-or-one inflated beta regression models. *Computational Statistics and Data Analysis*, *56*(6), 1609–1623. https://doi.org/10.1016/j.csda.2011.10.005

Payne, A. E., & Magnusdottir, G. (2015). An evaluation of atmospheric rivers over the North Pacific in CMIP5 and their response to warming under RCP 8.5. *Journal of Geophysical Research-Atmospheres*, *120*(21), 11,173–11,190. https://doi.org/10.1002/2015JD023586

PCIC (2013). Atmospheric rivers state of knowledge report. Pacific Climate Impacts Consortium,Victoria,BC. Retrieved from https://www.pacificclimate.org/sites/default/files/publications/Atmospheric%20Report%20Final%20Revised.pdf

Quick, M. C., & Pipes, A. (1977). U.B.C. watershed model. *Hydrological Sciences Journal*, *22*(1), 153–161. https://doi.org/10.1080/02626667709491701

Radić, V., Cannon, A. J., Menounos, B., & Gi, N. (2015). Future changes in autumn atmospheric river events in British Columbia, Canada, as projected by CMIP5 global climate models. *Journal of Geophysical Research-Atmospheres*, *120*(18), 1651–1669. https://doi.org/10.1002/2015JD023279

Ralph, F. M., Coleman, T., Neiman, P. J., Zamora, R. J., & Dettinger, M. D. (2013). Observed impacts of duration and seasonality of atmospheric-river landfalls on soil moisture and runoff in coastal northern California. *Journal of Hydrometeorology*, *14*, 443–459. https://doi.org/10.1175/JHM-D-12-076.1

Ralph, F. M., Dettinger, M. D., Lavers, D. A., Gorodetskaya, I. V, Martin, A., Viale, M., ... Cordeira, J. (2017). Atmospheric rivers emerge as a global science and applications focus. *Bulletin of the American Meteorological Society*, *98*(9), 1969–1973. https://doi.org/10.1175/BAMS-D-16-0262.1

Ralph, F. M., Neiman, P. J., Kingsmill, D. E., Ola, P., Persson, G., White, A. B., et al. (2003). The impact of a prominent rain shadow on flooding in California's Santa Cruz Mountains: A CALJET case study and sensitivity to the ENSO cycle. *Journal of Hydrometeorology*, *4*, 1243–1264. https://doi.org/10.1175/1525-7541(2003)004<1243:TIOAPR>2.0.CO;2

Ralph, F. M., Neiman, P. J., & Rotunno, R. (2005). Dropsonde observations in low-level jets over the Northeastern Pacific Ocean from CALJET-1998 and PACJET-2001: Mean vertical-profile and atmospheric-river characteristics. *Monthly Weather Review*, *133*, 889–910. https://doi.org/10.1175/MWR2896.1

Ralph, F. M., Neiman, P. J., & Wick, G. A. (2004). Satellite and CALJET aircraft observations of atmospheric rivers over the eastern North Pacific Ocean during the winter of 1997/98. *Monthly Weather Review*, *132*(7), 1721–1745. https://doi.org/10.1175/1520-0493(2004)132<1721:SACAOO>2.0.CO;2

Ralph, F. M., Neiman, P. J., Wick, G. A., Gutman, S. I., Dettinger, M. D., Cayan, D. R., & White, A. B. (2006). Flooding on California's Russian River: Role of atmospheric rivers. *Geophysical Research Letters*, *33*(13), L13801. https://doi.org/10.1029/2006GL026689

Reynoldson, T. B., Culp, J., Lowell, R., & Richardson, J. S. (2005). Fraser River basin. In A. C. Benke, & C. E. Cushing (Eds.), *Rivers of North America* (pp. 697–732). Amsterdam: Elsevier Inc.

Richardson, J. S., & Milner, A. M. (2005). Pacific coast Rivers of Canada and Alaska. In A. C. Benke, & C. E. Cushing (Eds.), *Rivers of North America* (pp. 735–773). Amsterdam: Elsevier Inc.

Rutz, J. J., Shields, C. A., Lora, J. M., Payne, A. E., Guan, B., Ullrich, P., et al. (2019). The Atmospheric River tracking method Intercomparison project (ARTMIP): Quantifying uncertainties in atmospheric river climatology. *Journal of Geophysical Research-Atmospheres*, *124*, 13,777–13,802. https://doi.org/10.1029/2019JD030936

Rutz, J. J., & Steenburgh, W. J. (2012). Quantifying the role of atmospheric rivers in the interior western United States. *Atmospheric Science Letters*, *13*(4), 257–261. https://doi.org/10.1002/asl.392

Rutz, J. J., Steenburgh, W. J., & Ralph, F. M. (2014). Climatological characteristics of atmospheric rivers and their inland penetration over the western United States. *Monthly Weather Review*, *142*(2), 905–921. https://doi.org/10.1175/MWR-D-13-00168.1

Rutz, J. J., Steenburgh, W. J., & Ralph, F. M. (2015). The inland penetration of atmospheric rivers over western North America: A Lagrangian analysis. *Monthly Weather Review*, *143*(5), 1924–1944. https://doi.org/10.1175/MWR-D-14-00288.1

Salathé, E. P. (2006). Influences of a shift in North Pacific storm tracks on western north American precipitation under global warming. *Geophysical Research Letters*, *33*(19), L19820. https://doi.org/10.1029/2006GL026882.

Santer, B. D., Mears, C., Wentz, F. J., Taylor, K. E., Gleckler, P. J., Wigley, T. M. L., et al. (2007). Identification of human-induced changes in atmospheric moisture content. *Proceedings of the National Academy of Sciences*, *104*(39), 15248–15253. https://doi.org/10.1073/pnas.0702872104

Shabbar, A., Bonsal, B., & Khandekar, M. (1997). Canadian precipitation patterns associated with the southern oscillation. *Journal of Climate*, *10*, 3016–3027. https://doi.org/10.1175/1520-0442(1997)010<3016:CPPAWT>2.0.CO;2

Sharma, A. R., & Déry, S. J. (2020). Variability and trends of landfalling atmospheric rivers along the Pacific coast of northwestern North America. *International Journal of Climatology*, *40*(1), 544–558. https://doi.org/10.1002/joc.6227

Spry, C. M., Kohfeld, K. E., Allen, D. M., Dunkley, D., & Lertzman, K. (2014). Characterizing pineapple express storms in the lower mainland of British Columbia, Canada. *Canadian Water Resources Journal*, *39*(3), 302–323. https://doi.org/10.1080/07011784.2014.942574

Stahl, K., Moore, R. D., & McKendry, I. G. (2006). The role of synoptic-scale circulation in the linkage between large-scale ocean-atmosphere indices and winter surface climate in British Columbia, Canada. *International Journal of Climatology*, *26*(4), 541–560. https://doi.org/10.1002/joc.1268

Stasinopoulos, D. M., & Rigby, R. A. (2007). Generalized additive models for location scale and shape (GAMLSS) in R. *Journal of Statistical Software*, *23*(7), 1–46. https://doi.org/10.18637/jss.v023.i07

Trubilowicz, J. W., & Moore, R. D. (2017). Quantifying the role of the snowpack in generating water available for run-off during rain-on-snow events from snow pillow records. *Hydrological Processes*, *31*(23), 4136–4150. https://doi.org/10.1002/hyp.11310

Tsonis, A. A. (2013). *An introduction to atmospheric thermodynamics*, (2nd ed.). New York: Cambridge University Press.

Viale, M., Valenzuela, R., Garreaud, R. D., & Ralph, F. M. (2018). Impacts of atmospheric rivers on precipitation in southern South America. *Journal of Hydrometeorology*, *19*(10), 1671–1687. https://doi.org/10.1175/JHM-D-18-0006.1

Vincent, L. A., Zhang, X., Brown, R. D., Feng, Y., Mekis, E., Milewska, E. J., et al. (2015). Observed trends in Canada's climate and influence of low-frequency variability modes. *Journal of Climate*, *28*, 4545–4560. https://doi.org/10.1175/JCLI-D-14-00697.1

Wang, T., Hamann, A., Spittlehouse, D. L., & Aitken, S. N. (2006). Development of scale-free climate data for western Canada for use in resource management. *International Journal of Climatology*, *26*(3), 383–397. https://doi.org/10.1002/joc.1247

Wang, T., Hamann, A., Spittlehouse, D. L., & Murdock, T. Q. (2016). ClimateWNA-high-resolution spatial climate data for western North America. *Journal of Applied Meteorology and Climatology*, *51*, 16–29. https://doi.org/10.1175/JAMC-D-11-043.1

Warner, M. D., Mass, C. F., & Salathé, E. P. (2015). Changes in winter atmospheric rivers along the North American West Coast in CMIP5 climate models. *Journal of Hydrometeorology*, *16*, 118–128. https://doi.org/10.1175/JHM-D-14-0080.1

Wentz, F. J., Ricciardulli, L., Hilburn, K., & Mears, C. (2007). How much more rain will global warming bring? *Science*, *317*(5835), 233–235. https://doi.org/10.1126/science.1140746

Werner, A. T., Schnorbus, M. A., Shrestha, R. R., Cannon, A. J., Zwiers, F. W., Dayon, G., & Anslow, F. (2019). A long-term, temporally consistent, gridded daily meteorological dataset for northwestern North America. *Scientific Data*, *6*(1), 1. https://doi.org/10.1038/sdata.2018.299–16

Wilks, D. S. (2011). *Statistical methods in the atmospheric sciences*, (3rd ed.). Amsterdam: Elsevier Inc.

Wilks, D. S. (2016). "The stippling shows statistically significant grid points": How research results are routinely overstated and overinterpreted, and what to do about it. *Bulletin of the American Meteorological Society*, *97*, 2263–2273. https://doi.org/10.1175/BAMS-D-15-00267.1

Wolter, K., & Timlin, M. S. (2011). El Niño/Southern Oscillation behaviour since 1871 as diagnosed in an extended multivariate ENSO index (MEI.Ext). *International Journal of Climatology*, *31*(7), 1074–1087. https://doi.org/10.1002/joc.2336

Zhang, X., Vincent, L. A., Hogg, W. D., & Niitsoo, A. (2000). Temperature and precipitation trends in Canada during the 20th century. *Atmosphere-Ocean*, *38*(3), 395–429. https://doi.org/10.1080/07055900.2000.9649654

Zhu, Y., & Newell, R. E. (1994). Atmospheric rivers and bombs. *Geophysical Research Letters*, *21*(18), 1999–2002. https://doi.org/10.1029/94GL01710

Zhu, Y., & Newell, R. E. (1998). A proposed algorithm for moisture fluxes from atmospheric rivers. *Monthly Weather Review*, *126*(3), 725–735. https://doi.org/10.1175/1520-0493(1998)126<0725:APAFMF>2.0.CO;2